DIPLOMARBEIT

Optimization of recombinant *Corynebacterium glutamicum* fed-batch processes

ausgeführt zum Zwecke der Erlangung des akademischen Grades eines Master of Science (MSc) unter der Leitung von

Prof. Dr. techn. Dipl.-Ing. Christoph HERWIG

betreut durch

Projektass. Dipl.-Ing. Daniel WALDSCHITZ

Institut für Verfahrenstechnik, Umwelttechnik und Technische Biowissenschaften

Technischen Universität Wien
Fakultät für Technische Chemie

von

Jakob KITZMÜLLER, BSc
[redacted]

Wien, am	Unterschrift des Betreuers	eigenhändige Unterschrift

Eidesstattliche Erklärung

Hiermit erkläre ich, dass ich diese Diplomarbeit selbstständig verfasst habe, dass ich die verwendeten Quellen vollständig angegeben habe und dass ich Zitate die anderen Publikationen im Wortlaut oder dem Sinn nach entnommen sind, unter Angabe der Herkunft als Entlehnung kenntlich gemacht habe.

Wien, am

eigenhändige Unterschrift

Abstract

The upcoming climate change as well as the resulting environmental problems pose serious challenges for mankind. This can be addressed in the field of biotechnology, for example, through the utilization of renewable precursors and waste materials. The majority of bioprocesses utilize first generation food crops as feedstock, limiting the availability of food for a steadily growing world population. Second generation raw materials, especially lignocellulosic biomass, could overcome these problems, by introducing circular economy and sustainability.

The European Union (EU) project iFermenter, to which this thesis contributes, is dealing with the biotechnological utilization of a waste product of the paper industry. The lignocellulosic byproduct spent sulfite liquor (SSL) is available in large quantities all over the world. However, a broad sugar pallet and inhibitors in the medium complicate application in industrial scale and limit the choice of microorganisms. One microorganism, that is capable of facing these challenges, is *Corynebacterium glutamicum*. However, in previous studies, only 5 - 10 % SSL in combination with a complex media was used for fermentation, which decreased the profitability and its contribution to sustainability. In this thesis, a recombinant *C. glutamicum* strain is used to utilize SSL as the sole carbon source for the production of pediocin PA-1, a high-value peptide with a specific activity against *Listeria monocytogenes*. Thereby, the optimal production conditions have to be identified, which is achieved in this work by investigating the limitation or excess of media components and by modeling of the biological behavior of the cells. For this purpose, the influence of SSL, nitrogen and phosphate availability on growth and pediocin titer in the induction phase was investigated via a Design of Experiment (DoE) approach. In order check if the obtained data can be further used in a model, the reliability was verified by assessing the elemental and electron balances. Finally, following these results, a mechanistic model was developed to identify the underlying mechanisms of the bacterium.

In this study, it was shown that the phosphate concentration has a significant influence on the pediocin titer in the reaction broth. With lower phosphate availability, higher pediocin titer were observed. In contrast, no significant influence of the DoE factors on growth was detected. One reason for this could be the fact that growth was considerably reduced in the induction phase.

The carbon and DoR balance meet the set acceptance criterion of ± 10 % recovery which demonstrates the fundamentals of both balances for SSL. However, the nitrogen and phosphorus balance did not meet this criterion and therefore, the corresponding data is not reliable and could not be further used. A model was established which is capable of accurately describing the uptake of the sugars mannose and xylose in batch but failed to predict the states biomass, glucose and acetate due to the high variability of the initial biomass. Moreover, the model accurately described the growth and uptake of mannose, xylose and acetate in fed-batch. However, the goal of identifying the underlying mechanisms of the product formation could not be reached due to the lack of a more precise analytical method.

In summary, it was shown that the phosphate concentration is an important factor for pediocin production by *C. glutamicum* on SSL. Furthermore, a mechanistic model was established that can accurately describe key parameters in the induced fed-batch. However, in order to improve the modeling of pediocin formation, a more precise method of determination needs to be developed in the future.

List of Abbreviations

Ace	Acetate
ANOVA	Analysis of variance
CEPI	Confederation of European Paper Industries
CER	Carbon evolution rate
CM	Chloramphenicol
CMA	Critical material attributes
CPP	Critical process parameter
CQA	Critical quality attribute
DCW	Dry cell weight
dO	Dissolved oxygen
DoE	Design of Experiment
DoR	Degree of reduction
EFSA	European food safety agency
ELISA	Enzyme-linked immunosorbent assay
EU	European Union
FDA	US Food and Drug Administration
FTIR	Fourier-transform infrared spectroscopy
Glc	Glucose
GRAS	Generally recognised as safe
HMF	5-hydroxymethylfurfural

HPLC	High performance liquid chromatography
ICH	International Conference of Harmonization
IPTG	Isopropyl-β-D-1-thiogalactopyranoside
LAB	Lactic acid bacteria
LoD	Limit of detection
Man	Mannose
MOPS	3-(N-morpholino)propanesulfonic acid
MPC	Model predictive control
NP	Nitrogen and phosphate feed
NRMSE	Normalized root mean square error
OD_{600}	Optical density at 600 nm
OUR	Oxygen uptake rate
Q2	Predictability
QbD	Quality by Design
P	Pediocin PA-1
R2	Model fit
RFU	Relative fluorescence unit
RQ	Respiratory quotient
SoF	Summary of fit
SSL	Spent sulfite liquor
StDev	Standard deviation
vvm	Volume air per volume liquid per minute
X	Biomass
Xyl	Xylose

List of Variables

c_i	$[\frac{g}{L}]$	Concentration of component i
$\overline{c_P}$	$[\frac{\mu g}{mL}]$	Mean of the product concentration
c_{SSL}	[%]	Concentration of spent sulfite liquor
D	$[\frac{1}{h}]$	Dilution rate
K_{Si}	$[\frac{g}{L}]$	Half-velocity constant of component i
l	[-]	Log likelihood
M_V	$[\frac{L}{mol}]$	Molar gas volume ≈ 22.41
n	[-]	Sample size
$n_{C/N}$	[-]	Molar ratio of carbon to nitrogen
$n_{C/P}$	[-]	Molar ratio of carbon to phosphorus
$n_{C/P,max}$	[-]	Maximum carbon to phosphate ratio
$n_{produkt}$	$[mol;\ e^-]$	Measured molar/electron quantities
n_{source}	$[mol;\ e^-]$	Molar/electron quantities provided to the system
q_{dO}	$[\frac{\mu g}{\mu g h}]$	Oxidation rate of pediocin at 15 % dO
q_P	$[\frac{\mu g}{g h}]$	Specific pediocin formation rate
$q_{P,max}$	$[\frac{\mu g}{g h}]$	Maximal specific pediocin formation rate
q_{S_i}	$[\frac{g_i}{g_X h}]$	Specific uptake rate of component i
$q_{S_i,max}$	$[\frac{g_i}{g_X h}]$	Maximal specific uptake rate of component i
$r_{balance}$	[-]	Balance ratio
r_i	$[\frac{g_i}{L h}]$	Volumetric rate of component i

r_{inert}	[-]	Inert gas ratio
S_i	$[\frac{g}{L}]$	Substrate concentration of component i
t	[h]	Time
t_{Inh}	[h]	Inhibition time
$\dot{V}_{in}$	$[\frac{L}{h}]$	Substrate inflow
V_R	[L]	Reactor volume
V_{sample}	[L]	Sample volume
x_i	[-]	sample entry
$\overline{x_i}$	[-]	Mean of sample entries
$x_{CO_2,Air}$	[%]	Carbon dioxide fraction air
$x_{CO_2,Offgas}$	[%]	Carbon dioxide in offgas
$x_{O_2,Air}$	[%]	Oxygen fraction air
$x_{O_2,Offgas}$	[%]	Oxygen in offgas
$\hat{y}$	[-]	Predicted y value
y_i	[-]	ith observation
$Y_{i/j}$	$[\frac{g_i}{g_j}]$	Yield of component i over j
γ_K	[-]	Collinearity index
$\hat{\Theta}$	[-]	Optimization criterion
μ	$[\frac{g_X}{g_X h}]$	Specific growth rate
$\overline{\mu}$	$[\frac{g_X}{g_X h}]$	Mean of the specific growth rate
μ_{max}	$[\frac{g_X}{g_X h}]$	Maximum specific growth rate
π	[-]	Circular number ≈ 3.14
σ	[-]	Variance

Contents

1 Introduction

1.1 General Field of Study

The earliest evidence of carried out bioprocesses by mankind date back to around 9000 B.C in China with the production of fermented beverages [1]. Over the centuries, various techniques have been developed to enhance and understand bioprocesses: selection of advantageous features, crossbreeding, DNA sequencing, non-directed mutagenesis, and now directed genome editing, most recently with the development of CRISPR/Cas9 in 2012 [2, 3]. These developments led to the rapid growth of biotechnology into a multi-billion dollar market, with further increases forecasted [4]. The different types of biotechnology, green, red and white, produce a broad palette of products from low-value food ferments or bulk chemicals over to high-value pharmaceuticals [5, 6].
The primary goal of industrial bioprocesses is to produce a high titer of the targeted product as inexpensively and quickly as possible and with the required product quality consistently [7]. In the pharmaceutical industry, the quality requirements of the products have been successively increased. However, since the process conditions can only be changed within rigid limits, fluctuating raw material quality, for example, leads to difficulties in maintaining the demanded quality [8]. Additionally, varying requirements and evaluation criteria are necessary for accession to different drug markets, prolonging and increasing the cost of the development process [9].

International Conference of Harmonization (ICH) was founded with the goal to harmonize the guidelines and requirements for pharmaceutical product registration to set global standards for quality, efficacy and safety [10]. The introduction of Quality by Design (QbD) shifts quality control from the final product to integrating quality into the process. The risk-based approach describes the design, analysis and control of critical process parameters (CPP) and critical material attributes (CMA) as well as critical quality attributes (CQA) in order to ensure product quality as well as enabling an adjustable and robust process [11]. The CQAs such as physical, (micro-) biological or chemical characteristics have a direct effect on the product. They have to be kept within a certain limit or range to ensure the required quality. Further, the CPPs and CMAs, for example, temperature or pH and particle size, have a direct impact on the

CQAs and should therefore be monitored or controlled throughout the process [12]. Design of experiment (DoE) and/or mathematic models are used to link the CPPs, CMAs and CQAs together within the design space in which the desired product quality can be provided within the boundaries of the space [9]. Movement within the design space is not considered as a change, which would require new approval by the authorities, and therefore, process adjustments can be carried out in order to respond to fluctuating raw material quality [12]. This gained flexibility allows a design and set up of a control strategy based on the obtained knowledge of the design space to ensure the product quality by controlling the CPPs based on the current CMAs in order to ensure constant CQAs [9]. Instead of performing excessive offline analysis, product quality is ensured by real-time release testing based on online process data [12].
Model-based approaches are used in all areas of pharmaceutical biotechnology, for example, experimental or process design, monitoring, predicting the dynamic behavior of the process or control, and therefore have the potential for a significant contribution to this field [13].

Modeling

Modeling in biotechnology is the generation and validation of mathematical representations which are capable of describing a bioprocess behavior or specific aspects of it [14]. The formulation of the model objective is a crucial step in the creation of a model and has to include the target values and the corresponding acceptance criteria [13]:

i) Model identification: The goal of model identification is to find and calibrate a model which can describe the relevant process observations. A complete understanding of the process can not be achieved, however, a certain process behavior can be described [15]. Model predictions are calculated based on input variables and mapped to real data. Depending on the deviations between these data, the hypothesis of the model is either disproved or confirmed [16]. Thereby, mechanistic can be identified as well as process observations and regulations of the cell can be understood [15].

ii) Off-line use: A validated model can be used to characterize strains. Thereby, the physiological model parameters are derived by fitting the model prediction to the observed growth curves, allowing a comparison of different strains [17]. DoE methods are used for systematic experiment planning and to obtain knowledge about the interactions of factors. Model-based approaches can be applied in order to reduce the amounts of experiments performed by reduction of the boundary values [18].

iii) Real-time use: Soft sensors and model predictive control (MPC) are widely applied for the real-time application of models in bioprocesses. Soft sensors are based on the first principle and use available online data such as off-gas composition or reactor inflows for monitoring or feedback control [19]. Process variables are determined which can not be directly measured or with a certain time delay, for example, specific

substrate uptake rates or biomass concentrations [20]. MPCs are used to predict the dynamic behavior of the process, determine the optimal operating points, and calculate the necessary control actions for the manipulatable variables, based on measured real-time data [21]. The system uses online data for recalculation which is performed in a defined interval or by specified process characteristics in order to react to process deviations. Therefore, the computations must be performed in real-time, which requires robust and fast algorithms [13].

In general, models are distinguished between two types: Mechanistic models are based on physical and biochemical principles [22]. These models require prior knowledge about the relationships and experimental data, however, they provide a transparent explanation of the observations. Problematic are non-identifiable parameters and especially the complexity of mechanisms of microorganisms which can only be simplified by the model and not fully described [23].
Data-driven models, on the other hand, describe relationships between input and output variables based on data sets with functions without a biological basis. Therefore, the model can only operate within the scope of the available data material, however, less prior knowledge is needed for setting up the model [23]. Data-driven models can only predict the mechanistic behavior of the process without providing an explanation of the underlying mechanism [24].

Analyzing the experimental data is an important task in order to generate a model which is capable of reflecting adequately the dynamic behavior of a bioprocess. Besides the evaluation of measurement inaccuracies and process-related influences, the reliability of the data for chemical processes can be determined by the evaluation of the elemental and electron balances [25]. Depending on which state variables are of interest for the implementation in the model, the corresponding balances, for example, carbon, nitrogen, sulfur or phosphorus balances, have to meet an acceptance criteria. A generated model has to be thoroughly tested if it reflects adequately the dynamic behavior of the process. Thereby, the simulated data of the model is compared to the experimental data and the model deviation is calculated [14]. Depending on the objective of the model, a predefined degree of fit is specified at which a successful validation of the model is given, for example, a normalized root mean square error (NRMSE) below 10 % [26] or 15 % [27].

Second Generation Feedstock

Recently, due to environmental problems, climate change and public pressure, the reduction of the dependency on fossil resources and instead the usage of renewable feedstocks are gaining more and more importance. Biorefinery processes address these challenges with the ability to utilize renewable feedstocks in order to produce (bulk-) chemicals, biofuels or energy and thus have the potential to introduce sustainability and cost-efficiency to industrial scale processes [2, 28]. The first generation of these bioprocesses uses food crops such as corn, grains, sugar beets or canola oil as en-

ergy sources, limiting the availability of food for the world's population. These raw materials are expensive and account significantly towards the price of the product, which is one of the major drawbacks in establishing profitability to bioprocesses and therefore, limits their scope of application. Additionally, biofuel production of first generation feedstock relies on government subsidies to maintain competitiveness and thus, is questioned to displace fossil resources [29].

These issues resulted in an increased interest in the usage of second generation raw materials for bioprocess application. Annually, about 150 billion tons of total biomass, combining both land and aquatic, are produced on earth, whereby food production only accounts for approximately 1.25 %, leaving a huge potential untapped [30]. These remaining broad range of non-food organic matter, such as wood- or agricultural residues, energy crops or lignocellulosic biomass, are usually thermally recycled, decayed or used in bioprocesses mainly to produce bulk chemicals (for example ethanol) [31].
However, this worldwide available feedstock could be used in sustainable processes as an alternative to fossil resources and could therefore serve as an important contributor in order to reduce greenhouse gas emission [32]. Additionally, the utilization of second generation feedstocks is in line with the European Union´s (EU) bioeconomy strategy "Innovation for Sustainable Growth", which aims to create a Green Europe and shape a target circular economy by 2030 [33]. Challenges include the availability of biomass throughout the year as well as the supply chain, fluctuating composition of the feedstock, process development, technical maturity and scale-up, which complicate a broad implementation [34]. A steadily increasing amount of second generation biomass is processed by the paper industry, generating large quantities of waste streams with unexploited capacity for bioprocesses [35, 36].

Spent Sulfite Liquor

In 2021, CEPI (Confederation of European Paper Industries) member countries utilized 112.3 million metric tons of wood for the production of 37 million tons of pulp [35]. There are mainly two chemical processes for pulp production: the Kraft process with a pre-extraction step and the acid sulfite process [37]. In the sulfite process, wood chips are delignified by cooking with acid sulfite/bisulfite salts resulting in solid cellulose, further used as pulp, and the pulp mill effluent, spent sulfite liquor (SSL). Cooking chemicals are regenerated in a recovery boiler and the remaining organic matter is typically incinerated to produce heat and power [38]. Nevertheless, the industrial waste stream has the potential to be a highly valuable feedstock for bioprocesses due to the huge availability of high quantities (approximately 90 billion liters worldwide, 1993) [36], cost-saving potential of raw materials and usage as a renewable substrate for circular economy [39]. The lignocellulosic waste stream media contains organic acids such as acetate as well as various fermentable sugar monomers, derived directly from the hydrolysis of hemicellulose without further pretreatment. Depending on the type of wood used for the sulfite process, the sugar composition varies significantly. Softwood leads to higher ratios of hexoses, mainly mannose and glucose [40]. In con-

trast, hardwood mostly yields the pentose sugar xylose, which accounts for up to 50 % of the total sugar in hardwood SSL [41]. This led to increased research work for organisms capable of metabolizing xylose in the waste media for ethanol production [41, 42]. In addition to the problems of varying sugar composition, SSL contains a multitude of inhibitory compounds, for example, organic acids, furfural, 5-hydroxymethylfurfural (HMF), phenols, and lignosulfonates. Various pretreatment methods were developed to either extract and further process compounds (for example: lignin- [43], phenolic components [44] and fermentable sugars) or to reduce undesired components and toxicity (for example filtration [45], over-liming [46] or steam stripping [47]). However, raising the number of process steps will increase the plant complexity and maintenance as well as the cost of the final product and should be kept to a bare minimum if feasible, in order to obtain economic efficiency [48]. High particle background complicates the development of inline sensors for sugar and biomass determination as well as offline biomass measurements with dry cell weight (DCW) and optical density at 600 nm (OD_{600}) [49, 50]. A fourier-transform infrared spectroscopy (FTIR) method was developed to detect the individual sugar concentrations of glucose, mannose and xylose by online measurements in a secondary feed-tank which allows to react to fluctuating raw material and to take actions to maintain optimal process conditions [51]. For estimating the biomass in the reaction broth, cell counting as well as flow cytometry are possible alternatives [49, 50].

In summary, chemicals produced from SSL have to compensate for the economic disadvantages associated with the development and operation of the rather complex bioprocesses on the waste media, as well as the otherwise generated energy from thermal incineration in pulp mills [52].

Modeling of Spent Sulfite Liquor

The development of models for bioprocesses with second generation raw materials is an important task to ensure broad application in industry. Although a number of publications examined the growth and production conditions of yeasts and bacteria on SSL, only a few addressed the development of kinetic models.

Inhibition of growth in SSL through the inhibitory compounds has been accounted for by general terms considering the SSL concentration in the reaction broth [53, 54] as well as by inhibitor-specific terms with the respective inhibitor concentration and inhibition constant [55]. The comparison of SSL with synthetic medium with the same sugar concentration with *Saccharomyces cerevisiae* showed that similar model parameters could be calculated. However, an inhibition term was introduced due to the inhibitors in the SSL which lead to a reduction of maximum growth rates and therefore, increased process time [55]. Individual sugar uptake rates and corresponding biomass yields of *Corynebacterium glutamicum* have been described for glucose, mannose and xylose [53, 56, 57, 58]. In these studies, the complex minimal medium

CGXII supplemented with 5 - 10 % (v/v) SSL has been used as a carbon source. However, the rather expensive complex media imposes an economic burden for up-scaled industrial processes. Further, an online monitoring strategy for biomass concentration and growth of *C. glutamicum* based on off-gas has been implemented for a batch and fed-batch cultivation [56].

Corynebacterium glutamicum

C. glutamicum is a non-pathogenic, facultative anaerobic, gram-positive bacterium that is very important for white biotechnology as a workhorse [59]. Especially for the production of the amino acids L-glutamate and L-lysine, the bacterium has been widely used in industrial scale for several decades [60]. Besides the production of platform chemicals and amino acids, *C. glutamicum* is further used for the recombinant production of over 70 compounds, including high-value proteins and peptides [61, 62].

First generation feedstocks such as sugarcane molasses, beet molasses or starch hydrolysates are typically processed as raw material depending on which carbon source is locally available [63]. Rather than utilizing these expensive food crops, the second generation of feedstocks, especially lignocellulosic biomass, for example, SSL, has the potential to serve as a renewable and cost-efficient raw material for fermentation with *C. glutamicum*. Simultaneous uptake of the most abundant sugars, glucose, mannose and xylose, is crucial for commercial application of the usage of SSL. The wild type of *C. glutamicum* is not capable to process xylose. However, genetically modified strains have been developed that are capable of a simultaneous uptake of glucose and xylose [64]. Furthermore, genetic modification of genes responsible for mannose uptake and catabolic pathway showed an improvement in mannose utilization as well as an achievement of a simultaneous uptake of mannose and glucose [65]. Several other advantages are a lipid-rich cell membrane, which increases the robustness of the bacteria [66], as well as tolerance against organic acids and aromatic media compounds [67]. In addition, *C. glutamicum* is capable of detoxifying furfural, a byproduct of lignocellulosic hydrolyzation which normally causes difficulties in its usage as a raw material for bioprocesses [68]. As a gram-positive bacterium, *C. glutamicum* has tremendous potential for secretory protein production due to the possibility of a direct release into the media and minimal protease activity [69, 70].

In summary, *C. glutamicum* is a promising candidate for the utilization of lignocellulosic waste materials. Moreover, introducing high-value products could further improve profitability and therefore, ensure an economical industrial process.

Bacteriocin

Antibiotics in clinical settings were a major breakthrough in modern medicine. Unfortunately, mis- and over-usage in livestock farming as well as in the treatment of diseases lead to a dramatic increase of antibiotic-resistant bacteria [71]. Additionally,

the discovery of antibiotics has declined since its peak in the mid-1950s, leading to the current antimicrobial resistance crisis [72].

A promising solution for the problem could be the replacement of antibiotics with bacteriocins, which occur in a broad range of bacteria, gram-positive and gram-negative, as well as archaea [73]. Bacteriocins are bioactive peptides or proteins which are non-detrimental for humans [74]. They are synthesized ribosomally and have antimicrobial activity against bacteria even at low concentration ranges (nanomolar range) [75]. Mostly, bacteriocins have a narrow range of action, advantageous in the competition for the same ecological niche with closely related organisms to the producer strain [76]. The mode of action is through growth inhibition or direct killing of the cells by targeting either cell membrane or cell functions [77, 78]. The producing cells possess immunity to the self-produced bacteriocin through a specific immunity protein [79]. Bacteriocin from lactic acid bacteria (LAB) draw special interest from the food industry due to the fact that these bacteria and their metabolites are generally recognized as safe (GRAS) [76]. For example, the bacteriocin nisin from *Lactococcus lactis* has the approval of the US Food and Drug Administration (FDA) as well as the European food safety agency (EFSA) and is used in several countries as a natural food preservative [80, 81]. Bacteriocins are used in a so-called hurdle technology for food safety and preservation: Different, mitigating approaches (involving physical, physicochemical and/or microbial steps), insufficient on their own, can in combination control or eliminate foodborne pathogens in food products and production [82, 83]. The pharmaceutical application of bacteriocins is limited by its production in natural producers growing on expensive, complex media, low production titers as well as high purification costs, which results in being sold as semi-purified preparations [84, 85, 86]. Therefore, the recombinant production of bacteriocins in microorganisms, capable of growing on low-cost and potentially renewable culture media, could increase economic viability and thus lead to broader uses.

Pediocin

Pediocin PA-1 belongs to class IIa bacteriocins [74]. PA-1 are small, heat-stable but oxygen-sensitive peptides produced by *Pediococcus spp.* [87, 88]. PA-1 possesses a highly specific activity against *Listeria monocytogenes*, a foodborne pathogen capable of surviving low pH, low temperatures and high somitic pressure, which is a particular threat against pregnant women, older people, immunosuppressed and infants [89, 90]. With a hospitalization rate of 92 % and a mortality rate of approximately 20 %, listeriosis, caused by the organism, is a serious threat [91]. Pediocin could provide an adequate prevention in food production systems as well as a potential alternative to antibiotic treatment of *Listeria* infections [92]. The recombinant production of pediocin could improve the product titer and purity of the product, using correspondingly less expensive precursors compared to the natural producer. Secondly, pediocin is a high-value product that could enable the usage of SSL as a feedstock beyond ethanol production [93].

1.2 Goals of this Study

Problem Statement

The utilization of the lignocellulosic waste product SSL in biotechnology enables the introduction of sustainability and circular economy. However, industrial application beyond ethanol production is hampered by inhibitors in the medium, the complex sugar composition and fluctuations of the material. One microorganism which is capable of facing these drawbacks is *C. glutamicum*. The shift to high-value products, for example, pediocin PA-1, could further enhance the profitability of using SSL as a feedstock. Thereby, the optimal process conditions have yet to be identified. For example, preliminary tests indicated that lower phosphate concentrations favor the pediocin PA-1 formation.
Current process and model developments of *C. glutamicum* utilize a mixture of SSL with complex media which compromises the economics of industrial scale production. This underlines the demand to develop processes that use SSL as the sole carbon source.

Novelty of the Approach

This work aims to develop and examine the feasibility of a process of *C. glutamicum* producing pediocin PA-1 with SSL as the sole carbon source without the addition of complex media or other additives. Furthermore, the elemental balances should be conducted to assess the reliability of the data as well as to examine if the fundamentals for SSL are valid. The experiments should be designed to identify the optimal process parameters by examining the impact of the sugar, phosphate and nitrogen availability on growth and product formation of the bacterium. Models of the bacterium growing on complex media with SSL addition are well established. In this contribution, the models are adapted to the current experiments with the goal to identify and reveal the biological mechanistics of the cell.

Goals of the study

The main objective of this work is to optimize pediocin titer in a bioprocess of *C. glutamicum* utilizing SSL as the sole carbon source by

i) checking the reliability of the experimental data and the fundamentals of balancing on SSL through assessing the elemental balance with an acceptance criterion of 10 % [26].
ii) Upon validation, the influence of SSL, nitrogen and phosphate availability on growth and product formation in the induction phase is determined.
iii) Subsequently, a model is set up and adapted to the performed experiments in order to identify the underlying model of the process observations (biomass, sugars, acetate and pediocin). The model should be validated by examining the time-resolved values, observed vs. predicted plots and an NRMSE of less than 15 % [27].

2 Materials and Methods

2.1 Strain

For this study, the engineered strain *Corynebacterium glutamicum CR099::U pXMJ19-pedACD*, provided by the university of Ulm, was used [86]. *C. glutamicum CR099* is a descendant of the wildtype *C. glutamicum ATCC 13032* in which insertion sequences and prophages were deleted [94], resulting in increased genome- and plasmid stability [95]. *C. glutamicum CR099* displays resistance against pediocin PA-1 with no affection on growth at 2 μg mL^{-1} and no growth restriction up to 12.5 μg mL^{-1} [86]. *pedACD*^{Cg} is ligated to the *pXMJ19 vector* under a T7-promoter, which is inducible with Isopropyl-β-D-1-thiogalactopyranoside (IPTG). The expressed compound is equivalent to pediocin PA-1 in size and mass with activity against *Listeria monocytogenes* and *Listeria innocua* [86]. The synthetic *pedACD*^{Cg} operon consists of three genes: the structural gene *pedA* encodes for the precursor of pediocin PA-1, *pedC* and *pedD* for proteins which are required for processing, cleavage and segregation of the bacteriocin [96]. Additionally, genes for xylose metabolization (pEKEx3-xylAB) and enhanced mannose uptake (pVWEx1-manA) are introduced into the genome of the engineered strain compared to a similar strain in [56] with the genes on plasmids.

2.2 Raw material

SSL was sourced from Borregaard (Sarpsborg, Norway). Three different batches were used for this study whereby the concentration ranges are shown in table 2.1. Analysis of the SSL used for this study showed that the media supplies most of the nutrients required for bacterial growth except a source for nitrogen and phosphate. Additionally, the media contains high levels of Ca^{2+}. Preliminary tests showed that the amount of phosphate required for bacterial growth lead to precipitation in the media. One reason for this could be the formation of $Ca_3(PO_4)_2$. Therefore, the necessary quantities of nitrogen and phosphate were provided by external feeding of urea and KH_2PO_4.

Table 2.1: Substrate concentration range of the SSL batches used for this study

Glucose [g/L]	Mannose [g/L]	Xylose [g/L]	Acetate [g/L]
43 - 46	138 - 183	60 - 65	6.1 - 6.7

2.3 Experimental Plan

In order to determine the effects of SSL, nitrogen, and phosphate on cell growth and pediocin titer, experiments consisting of a batch followed by an induced two-feed system were carried out. The batch phase was performed with the same conditions for each experiment. The required amount of nitrogen and phosphate for this phase were supplemented by an initial volume and a nitrogen/phosphate feed (NP) consisting of urea and KH_2PO_4. In fed-batch, various concentrations of nitrogen, phosphate and SSL were supplied externally with an exponential feed ramp of $\mu = 0.03$ h^{-1} over a time period of 30 - 32 h respectively. These conditions were selected to correspond to a 3-factor 2-level full factorial DoE with a triplicate center point (Figure 2.2). The response values growth and pediocin titer were examined in this design. The following factors and boundaries were applied, whereby n_C/n_N and n_C/n_P correspond to the ratio of the amount of carbon to nitrogen and phosphates, respectively:

i) c_{SSL} (Levels: 25 %; 37.5 %; 50 %)

ii) n_C/n_N (Levels: 1/5; 1/7.5; 1/10)

iii) n_C/n_P (Levels: 1/15; 1/30; 1/45)

The boundaries were chosen in order to investigate different influences of the factors. The limits (25 % SSL, 1/5 n_C/n_N and 1/15 n_C/n_P) were set according to the conditions in the batch phase. For the upper limit of SSL, the concentration was doubled which results in more available sugars for the cells but at the same time an increased concentration of inhibitory compounds. The sugar to nitrogen ratio was lowered in order to examine the impact on growth. Previous experiments indicated a higher product titer when performing a fed-batch with an exponential feed ramp, but with constant feeding of NP. This leads to less available nitrogen and phosphate over the course of the process for the proliferating cells. In order to investigate this hypothesis, the ratio of sugar to phosphate was divided into thirds in order to severely limit the available phosphates for the cells.

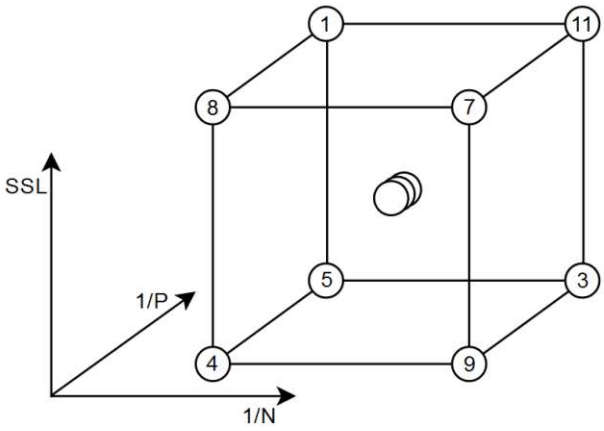

Run Order	SSL [%]	n_C/n_N	n_C/n_P
1	50	5	45
2	37.5	7.5	30
3	25	10	45
4	25	5	15
5	25	5	45
6	37.5	7.5	30
7	50	10	15
8	50	5	15
9	25	10	15
10	37.5	7.5	30
11	50	10	45

Table 2.2: Overview of the DoE conditions.

2.4 Cultivation

Preculture

C. glutamicum CR099::U pXMJ19-pedACD glycerol cryo-stock (stored at -80 °C) was streaked onto 2TY-agar plates (Tryptone 16 g L^{-1}; yeast extract 10 g L^{-1}; NaCl 5 g L^{-1}; chloramphenicol (CM) 12 μg mL^{-1} ; agar agar 18 g L^{-1}), incubated [30 °C ; 48 h] and stored at 4 °C for further usage. 2 x 12.5 mL 2TY in 15 mL reaction tubes were inoculated with single colonies of the agar plate and incubated [30 °C; 230 rpm; 24 h]. The preculture was transferred to 1 L shake flasks containing 225 mL 2TY and 25 mL SSL with 100 g L^{-1} 3-(N-morpholino)propanesulfonic acid (MOPS) and incubated [30 °C; 230 rpm; 24 h].

Reactor setup

The cultivation experiments were performed with a stirred bioreactor system (Labfors 5, Infors, Switzerland) with a maximum working volume of 3.5 L. pH was monitored with a potentiometric pH sensor (Hamilton, Switzerland) and controlled at 7.0 by the addition of 2.5 M KOH and 2.5 M H_2SO_4. Dissolved oxygen (dO) was measured with a dO probe (Hamilton, Switzerland) and maintained above the setpoint with 0.3 vvm and an adaption of stirrer speed (400 to 1200 rpm). The O_2 and CO_2 fractions of the exhaust gas were analyzed with an off-gas analyzer (BlueInOne Cell, BlueSens gas sensor GmbH, Germany). Samples (approximately 25 - 35 mL) were taken every 3 hours automatically by an auto sampler (custom-made by the research group) and stored at 4 °C until analysis. A visualization of the experimental setup is shown in figure 2.1.

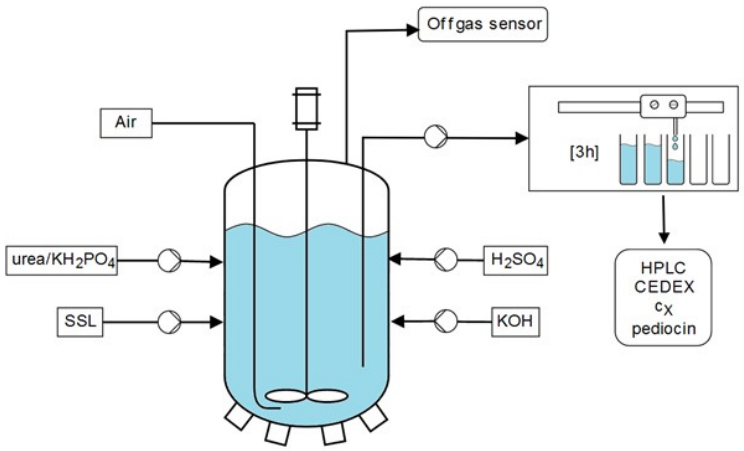

Figure 2.1: Experimental setup of the batch/fed-batch fermentation. SSL, NP feed, acid and base were supplied via external feeding. The aeration was performed with air and the offgas was analyzed externally. Samples were taken every 3 h and analyzed for sugar, biomass and product concentration.

Batch

1 L 25 % SSL, supplemented with 10 mL L^{-1} antifoam (20 % polypropylene glycol) and 12 μg mL^{-1} CM, was used as carbon source for the batch phase of the fermentation. 20 mL of NP feed (112.5 g L^{-1} urea and 170 g L^{-1} KH_2PO_4) were added as an initial bolus shot. An appropriate inoculation volume (approximately 50 - 65 mL) was chosen to achieve an initial OD_{600} of 1 - 1.2 in the reactor which is equal to approximately 0.23 - 0.28 g L^{-1}. The dO setpoint was set to 30 % and NP feed (112.5 g L^{-1} urea and 170 g L^{-1} KH_2PO_4) was fed over 12.5 h (94 mL; $\dot{V}$ = 7.5 mL/h). At the beginning of a process of *C. glutamicum* on SSL, the bacterium detoxifies inhibitors in the SSL which leads to a phase with strongly reduced growth [68]. The end of batch, approximately after 26 h, was detected with a corresponding drop of the CO_2 and dO signal, indicating a drop of metabolic activity.

Fed-batch

Depending on the experiment performed, different concentrations of 1.5 L SSL and 220 mL NP feed were prepared according to the experimental plan (Section 2.3). 10 mL L^{-1} antifoam, 12 μg mL^{-1} CM and 47.67 μg mL^{-1} IPTG were supplemented to the SSL. For the highest KH_2PO_4 concentrations (experiments 7 and 8), the feed volume as well as the feed rate were doubled to ensure solubility. In order to induce the process, 47.67 μg mL^{-1} IPTG were added to the reaction broth. Afterwards, the feeds SSL ($\dot{V}_0$ = 30 mL/h; μ = 0.03 h^{-1}; 30 - 32 h) and NP ($\dot{V}_0$ = 30 mL/h; μ = 0.03 h^{-1}; 30 - 32 h) were started and the dO setpoint was lowered to 15 %.

2.5 Samples

DCW measurements were conducted by centrifugation (12,000 g, 10 min, 4 °C) of 3 x 1.8 mL culture broth, whereby the supernatant was used for the analysis the sugars, organic acids and pediocin. The precipitate was dried at 120 °C for 72 h and gravimetrically determined in order to track the amount of precipitate throughout the process. Pre-tests showed that the biomass concentration can not be determined via OD_{600} or DCW measurements due to precipitation formed in the reaction broth. However, biomass concentration was determined by measuring the fluorescence and estimating the value against a standard (*C. glutamicum CR099::U pXMJ19-pedACD* cultivated in 2TY; biomass measurement via DCW). Therefore, 1 mL cultivation broth was centrifuged (3200 rpm, 10 min, 4 °C), the cell pellet was washed, resuspended with 1 mL 0.9 % saline solution and relative fluorescence units (RFU) were measured (excitation 280/10 nm; Emission: 340/20 nm) with a plate reader (Infinite M200 PRO, TECAN, Switzerland).

For sugar analysis, particle-free reaction broth was diluted 1:20 and measured with high performance liquid chromatography (HPLC UltiMate 3000, Thermo Fisher, USA) with a lead column (Nucleogel Sugar Pb, Macherey-Nagel GmbH, Germany). Therefore, a flow rate of 0.4 mL/min deionized water at a temperature of 79 °C and detection via a refractive index detector (RI-100, Shodex, USA) was applied. Acetate, glutamate, lactate, ammonia and phosphate concentrations of the broth were determined via a photometric analysis of enzymatic reactions (Cedex Bio HT Analyzer, Roche, Switzerland) of the supernatant.

The bacteriocin activity of the particle-free reaction broth was examined with a standard microtiter plate assay according to [86] with the indicator strain *L. monocytogenes EGDe/pNZ44*. Pediocin concentrations were determined by comparison of a two-fold dilution series of the reaction broth with a pediocin standard in 96 well plates in which at least 50 % growth inhibition of the indicator bacteria occurs (The biomass concentration was detected via OD_{600} with a plate reader (Infinite M200 PRO, TECAN, Switzerland)). Therefore, a multiple of 0.5 of the applied standard can be detected by the assay.

2.6 Data Analysis

The data of the experiments were collected by the process information management software Lucculus (Securecell, Switzerland). Data evaluation and modeling were carried out with Matlab 2022a (Mathworks, USA). MODE 11 (Umetrics, Sweden) was used for the assessment of the DoE.

Respiratory rates

The oxygen uptake rate (OUR), carbon evolution rate (CER) and respiratory quotient (RQ) were calculated with formula 2.1 - 2.3.

$$r_{O_2} = OUR = -\frac{\dot{V}_{in} \cdot (x_{O_2,Air} - r_{inert} \cdot x_{O_2,Offgas})}{M_V} \left[\frac{mol}{h}\right] \tag{2.1}$$

$$r_{CO_2} = CER = \frac{\dot{V}_{in} \cdot (r_{inert} \cdot x_{CO_2,Offgas} - x_{CO_2,Air})}{M_V} \left[\frac{mol}{h}\right] \tag{2.2}$$

$$RQ = \frac{CER}{OUR} [\,-\,] \tag{2.3}$$

Volumetric and specific rates

The volumetric rate was determined with formula 2.4 and the specific rates with formula 2.5.

$$r_i = \frac{\Delta c_i}{V_R \cdot \Delta t} \left[\frac{g_i}{Lh}\right] \tag{2.4}$$

$$q_i = \frac{r_i}{c_X} \left[\frac{g_i}{g_X h}\right] \tag{2.5}$$

Estimation of sample Volume

A sample was taken every 3 h, resulting in an average of 24 samples per process. Assuming a volume of approximately 30 mL per sample, this amounts to 720 mL that were withdrawn over the time course of the process. With a batch volume of 1 L and a fed-batch volume of 1.5 L, this would result in a total loss of approximately 30 % reactor volume and would have therefore a substantial influence on the process evaluation, especially the elemental balances. The taken reaction broth volume, consisting of discarded waste and sample, varied between the processes and no uniform sample volume could be determined. Therefore, each sample volume was calculated individually. The reactor volume before and after the sampling time was interpolated in order to include volume increase due to feeding. Sample volume was determined by calculation of the difference of the interpolations at the sample time point, illustrated in figure 2.2.

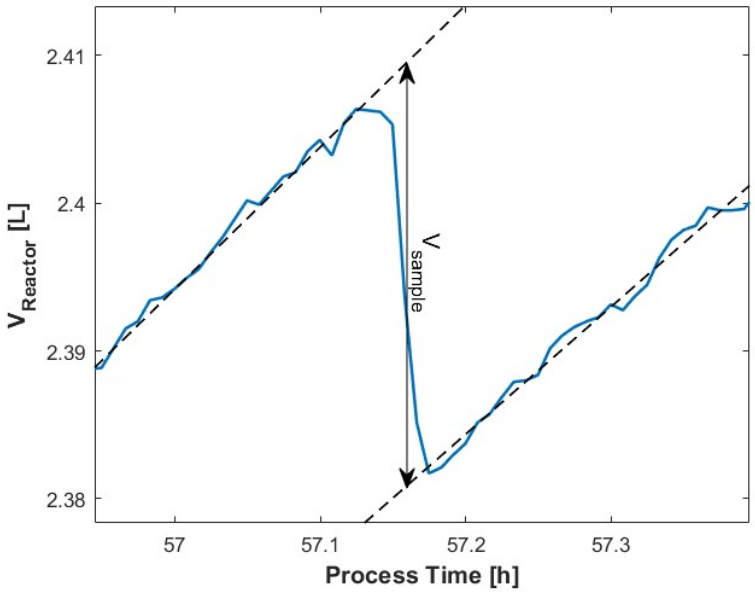

Figure 2.2: Estimation of the sample volume by interpolation of the reactor volume before and after the sample. The sample volume is determined by calculating the difference between the two interpolations at the sample time.

Elemental Balance

The balances were calculated according to the general equation of the reaction (equation 2.6). The sugars (glucose, mannose, xylose) and organic acids (acetate, lactate and glutamate) were summarized as SSL. The volume loss due to sampling is taken into account as the variable sample. The elemental biomass composition from *C. glutamicum* in the exponential growth phase was adopted from [56]. As a simplification, this composition was further used for the calculation of the induced phase, since the biomass content is low compared to the overall quantities present in the taken samples. The biomass has a molecular weight of 27.78 g $Cmol^{-1}$ with an average elemental composition of:

$$C_1H_{1.832}N_{0.176}O_{0.615}P_{0.0157}S_{0.0033}K_{0.0005}Mg_{0.0005}Ca_{0.0058}Na_{0.0267}Cl_{0.0034}$$

Pre-tests showed that a precipitate is formed throughout the process which consists of biomass and other unknown components. With the introduction of $Ca_3(PO_4)_2$ as a secondary component of the DCW, the P-balance could be improved compared to the balance without this simplification.

$$\begin{aligned} O_2 \ + \ SSL \ + \ urea \ + \ PO_4 \ \longrightarrow \\ CO_2 \ + \ SSL \ + \ urea \ + \ NH_3 \ + \ PO_4 \ + \ X \ + \ sample \end{aligned} \tag{2.6}$$

The balance ratio (equation 2.7) indicates how accurate the elemental balance is at a given sample time point, whereby a value of 1 reflects perfect balancing and a low deviation throughout all processes good robustness. In order to implement the examined balance into the model, it has to meet the set critical acceptance criterion of 10 %.

$$r_{balance} \ = \ \frac{\sum_{i=1}^{k} n_{produkt,i}}{\sum_{j=1}^{l} n_{source,j}} \tag{2.7}$$

2.7 Model-Analysis

The mechanistic model as well as the model analyzing scripts were programmed in Matlab 2022a. The model parameters were estimated using an algorithm based on log likelihood (l) (equation 2.8) with the sample size n, the variance σ, the sample entry x_i and the mean of the sample entries $\overline{x_i}$. The log likelihood was calculated for each sample entry individually (n = 1). As an optimization criterion ($\hat{\Theta}$), the minimization of the mean of the negative log likelihood (equation 2.9) of the estimated and observed model states were applied, following the same setup as in [97].

$$l = -\frac{n}{2} \cdot ln\left(2\pi\right) - \frac{n}{2} \cdot ln\left(\sigma^2\right) - \frac{1}{2\sigma^2}\left(x_i - \overline{x_i}\right) \tag{2.8}$$

$$\hat{\Theta} = arg\ min\ \left(\ mean\left(-l\right)\right) \tag{2.9}$$

Tuning of the parameters was performed by applying subsets of the parameters to the algorithm. According to [98], poor identifiability of the parameter subset is given when the collinearity index γ_K is greater than 15.
Important for the estimation of the process parameters is an appropriate error range of the states to tell the model how far the real value can deviate from the measuring point. This allows the model to account for measurement uncertainty and improve the fit to relevant data, rather than relying on data that in reality has high measurement noise [99]. The possible value range and measured error range of the states are shown in table 2.3. The high error of pediocin measurement originates from the applied assay

which can only detect the component in a dilution series, whereby the next higher value is double whereas the lower one is half of the measured value resulting in an error of +100/-50 %.

Table 2.3: Value and error range of states

	Value range	Error range
Biomass	0.23 - 3 g/L	0.3 g/L
Glucose	0 - 17.3 g/L	0.5 g/L
Mannose	0 - 61.7 g/L	0.5 g/L
Xylose	0 - 24.5 g/L	0.5 g/L
Acetate	0 - 2.8 g/L	10 mg/L [100]
Pediocin	0 - 4 μg/mL	+100/-50 % [86]

For the analysis of the model, different approaches were applied: The model states of single experiments were simulated and compared with the experimental data. Multiple experiments were evaluated with observed vs. predicted plots and by the calculation of the NRMSE (equation 2.10) of the model states of all samples as well as the corresponding standard deviations in order to assess the performance of the model and the reproducibility.

$$NRMSE = \frac{\sqrt{\frac{\sum(\hat{y}-y_i)}{n}}}{mean\,(y)} \tag{2.10}$$

3 Results and Discussion

In this chapter, the results of the conducted processes are shown. First, the concentration profile of relevant process states, the evaluation of gas rates as well as the specific rates of an exemplary process, elemental balances and the DoE results are presented. Second, the applied mechanistic model kinetics and differential equations are shown as well as the model analysis for batch and fed-batch separately, consisting of time-resolved values of a single process, observed vs. predicted plots and NRMSE analysis.

3.1 Process Evaluation

3.1.1 Concentration Profile

Important process states throughout an exemplary process are shown in figure 3.1. The biomass concentration of 0.25 g L^{-1} at the beginning of the process corresponds to the calculated concentration through the applied inoculum. The concentration increases slightly to about 0.5 g L^{-1} after 9.5 h and with a following, faster increase to 1.4 g L^{-1} until the end of the batch. In fed-batch, the biomass concentration decreases until the end of the process. In the batch phase, the cells grow exponentially. However, growth is reduced in the induced fed-batch due to the metabolic burden of product formation, leading to dilution due to increasing reactor volume.

The glucose concentration decreases in the batch phase to approximately 3 g L^{-1}. The end of batch was predefined as a complete uptake of glucose by the bacteria which was considered as a drop in the CER signal. However, the concentration plot shows that glucose is still remaining in the reaction broth when the feeding was started. One reason for this could be the complete consumption of acetate leading to a reduction of CER. In fed-batch the glucose concentration increases till the end of feeding due to overfeeding and decreases in the phasing out phase of the process. Mannose and xylose concentrations decrease in batch by the uptake through the cells. In fed-batch, both sugar concentrations in the reaction broth increase due to overfeeding. After the end of feeding, the concentrations decrease.

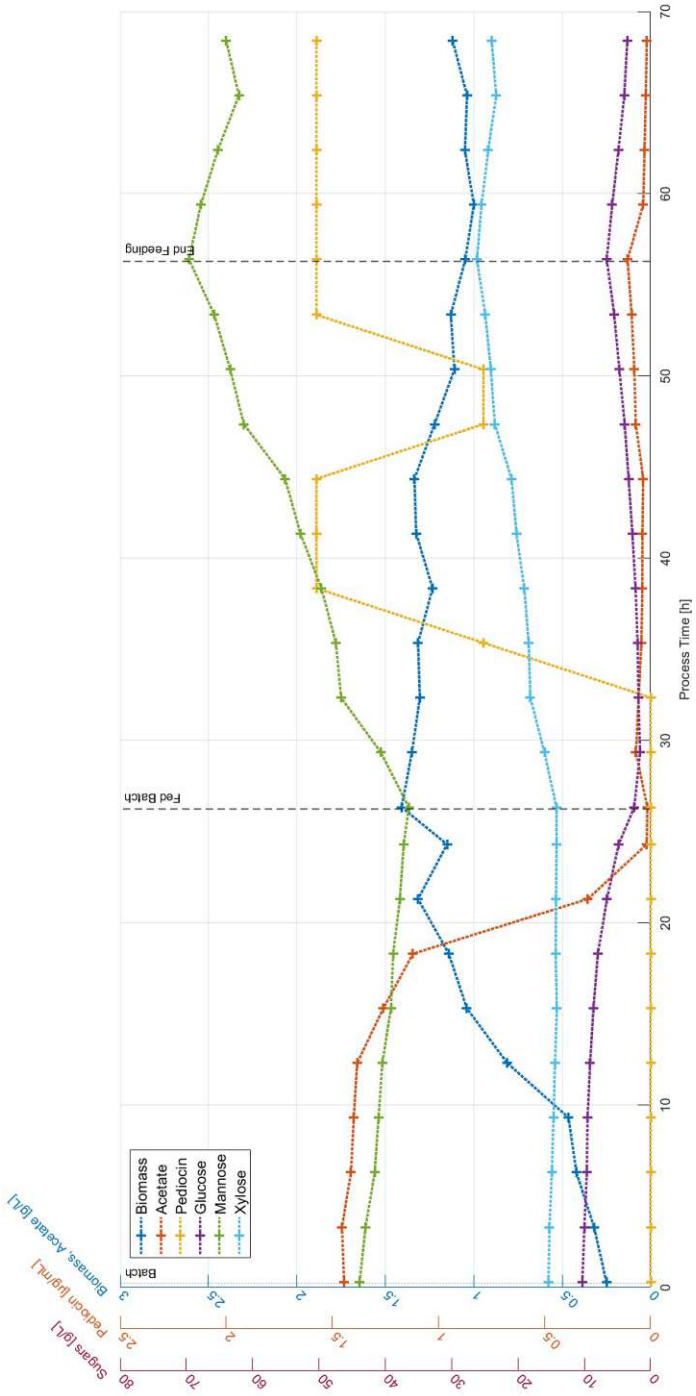

Figure 3.1: The course of the concentration profile of an exemplary experiment over the process time. Exponential growth occurs in the batch, however, in fed-batch the concentration decreases because of the metabolic burden of the induction. The sugar concentrations increase in the fed-batch due to overfeeding.

The acetate concentration is around 1.75 g L^{-1} until approximately 12 h process time and afterwards, the organic acid is completely utilized by the cells over a time period of 12 h. This indicates that the acetate uptake is inhibited in the beginning of the process. In fed-batch, the acetate concentration levels off to around 0.05 - 0.1 g L^{-1} with a slight increase to the end of the feeding phase. The evaluation of all performed experiments showed, that the acetate concentrations increase in the fed-batch when a DoE factor of 37.5 and 50 % SSL were applied, which was caused by overfeeding of the bacteria with the waste media.

The pediocin titer increase after approximately 5 h in the induced fed-batch phase to approximately 1.58 μg mL^{-1}. At around 48 h the concentration decreases to 0.8 μg mL^{-1} and after 6 h increases to 1.58 μg mL^{-1} forming a step formation. After the end of feeding, the pediocin concentration remains at 1.58 μg mL^{-1}. The decrease of the titer is caused by measurement inaccuracies due to the high error rates of the assay. The maximum level of pediocin in the reaction broth is reached after approximately 12 h fed-batch. In order to increase the space-time yield and save resources in industrial production, a reduction of the fed-batch time is beneficial if the maximum product concentration can be maintained. However, to determine this maximum, more accurate measurement methods are necessary, for example, a HPLC method or an enzyme-linked immunosorbent assay (ELISA). Furthermore, an adequate prediction tool is advantageous in order to determine the time to stop the fermentation.

3.1.2 Respiratory Rates

The respiratory rates of an exemplary process are shown in figure 3.2. In general, only a low OUR and CER are observed in the initial phase of the process. After about 12 h, the rates increase/decrease exponentially which coincides with the onset of acetate uptake (section 3.1.1). Respiratory rates drop at approximately 22 h, which was assumed to be complete consumption of glucose whereas complete uptake of acetates occurred during this period. Therefore, the end-of-batch criterion needs to be re-evaluated, for example, whether a second drop is visible in the rates due to complete glucose uptake or implementation of a rapid glucose measurement method such as CEDEX or blood glucose meter.

The feeding was started at approximately 26 h process time which leads to an increase/decrease of the respiratory rates. As the fed-batch progresses, the rates decrease slightly, caused by a decreasing biomass concentration in the reaction broth. After the end of feeding, the rates drop and decrease till the end of the process due to reduced substrate availability. In fed-batch, the RQ stabilizes at a constant level of approximately 1.3, indicating a stable metabolic activity of the bacteria.

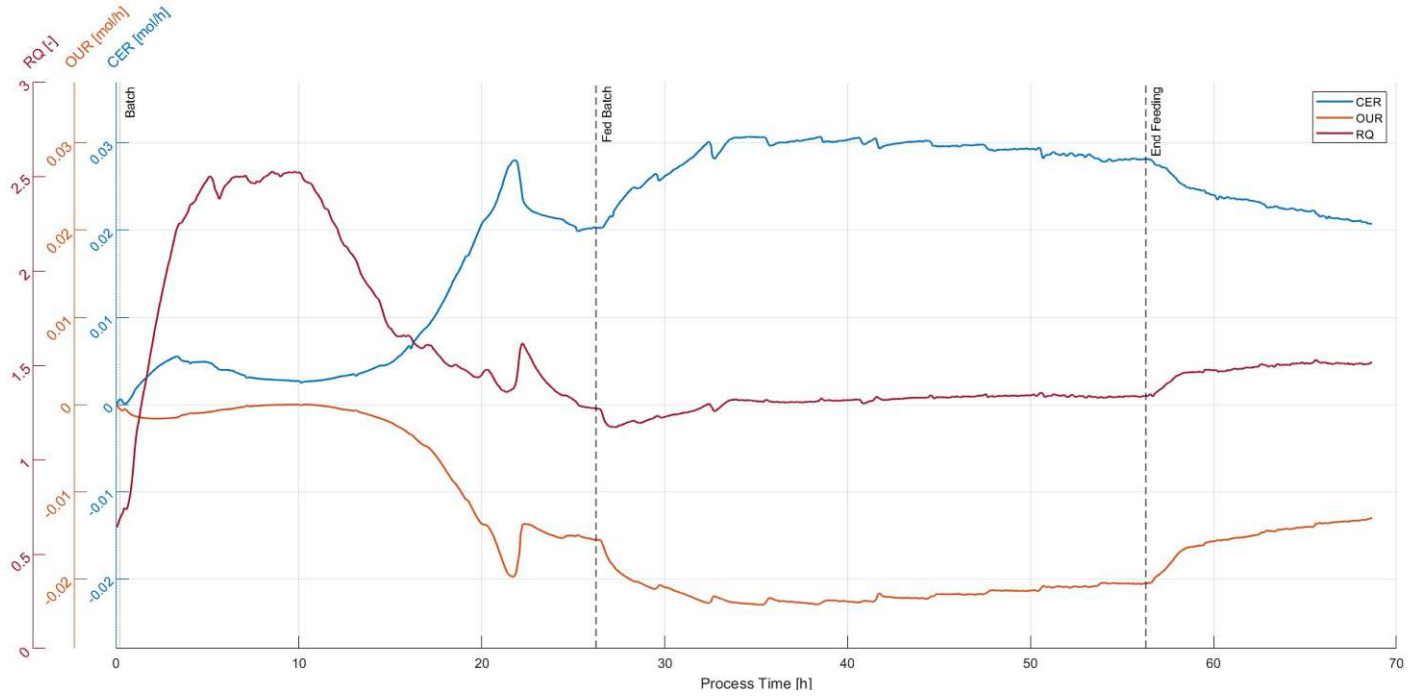

Figure 3.2: The respiratory rates OUR, CER and RQ over process time. It was assumed that the complete consumption of glucose at approximately 22 h, corresponding to the end of the batch, would be indicated by the drop in the CER signal. However, this drop was caused by the complete uptake of acetate, which leads to glucose still be present in the reaction broth.

3.1.3 Specific Rates

The specific rates and the corresponding concentrations of an example process are displayed in figure 3.3 - 3.6. It is seen in figure 3.3, that the biomass concentration increases sharply until the end of the batch. The specific growth rates are at approximately 0.06 h^{-1} and decrease at the end of the batch. The significant negative specific growth rate of -0.55 h^{-1} immediately before the start of the fed-batch derives from the drop in biomass concentration which is caused by an outlier of the biomass determination. As reported in [68], the maximum specific growth rate of *C. glutamicum ATCC13032* is reduced under aerobic conditions in the presence of furfural. Further, the bacterium is capable of the detoxification of furfural [68]. Depending on the furfural concentration in the SSL, the specific growth rate is therefore reduced at the beginning of the process and rises throughout the detoxification. However, the specific growth rates were not significantly reduced in the early stages of all conducted experiments. Since the furfural concentration of the SSL is not available, measurements should be carried out in order to assess a possible growth reduction. In the fed-batch, the specific growth rates are low leading to a decrease in the biomass concentration in the reaction broth due to dilution. The growth is substantially reduced compared to the early stages of the process and does not meet the applied growth rate of 0.03 h^{-1} of the exponential feed ramp. This reduced growth is caused by the metabolic burden of protein overexpression in the induction phase [101].

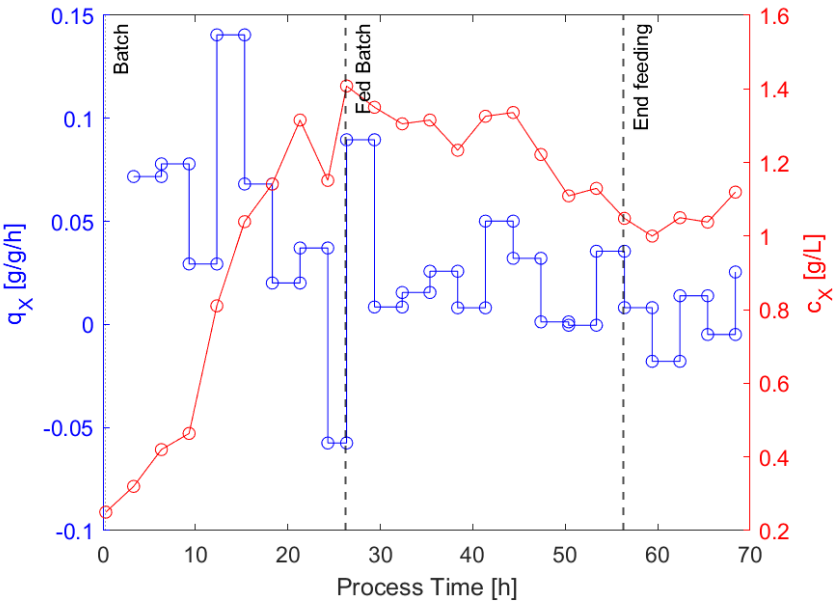

Figure 3.3: Specific growth rate and biomass concentration over process time.

As seen in figure 3.4, the glucose concentration decreases exponentially until the end of batch due to the increasing biomass. The specific substrate uptake rate are at approximately 0.35 g g^{-1} h^{-1} in the beginning of the process and decrease after around 10 h process time to 0.15 g g^{-1} h^{-1}. Afterwards, the specific rate increase to a maximum of approximately 0.95 g g^{-1} h^{-1} at end of batch. One reason for this could be that the acetate uptake inhibits the glucose uptake, leading to increased glucose uptake rates when acetate is completely consumed at approximately 24 h process time. In fed-batch, the specific uptake rate steadily decreases. One reason for this could be that the pediocin titer in the reaction broth increases in the fed-batch.

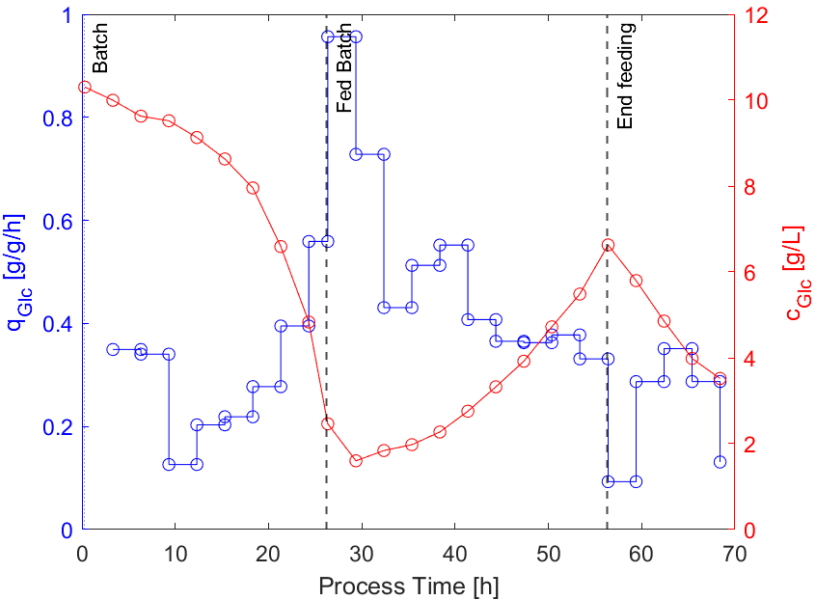

Figure 3.4: Specific glucose uptake rate and glucose concentration over process time.

Mannose and xylose concentrations (figure 3.5 - 3.6) decrease steadily in the batch phase, increase in the fed-batch due to overfeeding and decrease after the end of feeding. The corresponding uptake rates decrease until the end of batch. In fed-batch, the rate fluctuates to negative values which are caused by inaccuracies in the HPLC sugar measurements. Therefore, it can not be assessed whether the specific rates remain constant or decrease towards the end of the fed-batch.

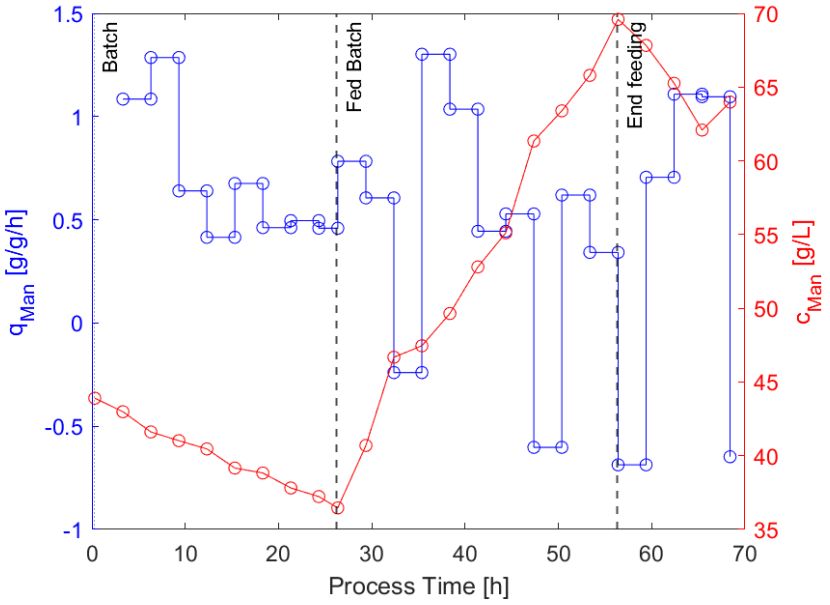

Figure 3.5: Specific mannose uptake rate and mannose concentration over process time.

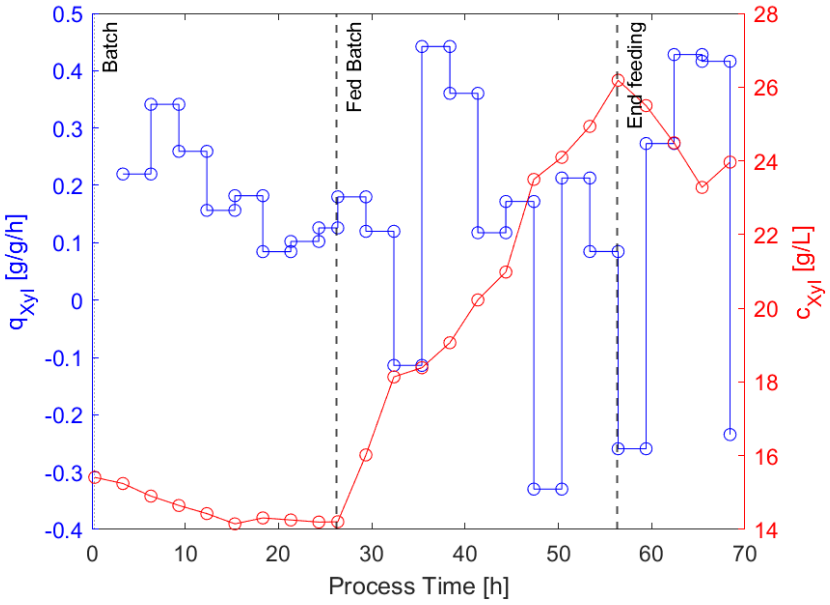

Figure 3.6: Specific xylose uptake rate and xylose concentration over process time.

The acetate concentration and specific uptake rate are displayed in figure 3.7. The uptake rate is low at the beginning of the batch, indicating an inhibition of the uptake. The specific rate peaks at approximately 22 h leading to the complete consumption of acetate in the reaction broth. In fed-batch the uptake rate levels off to around 0.9 g g^{-1} h^{-1} on average.

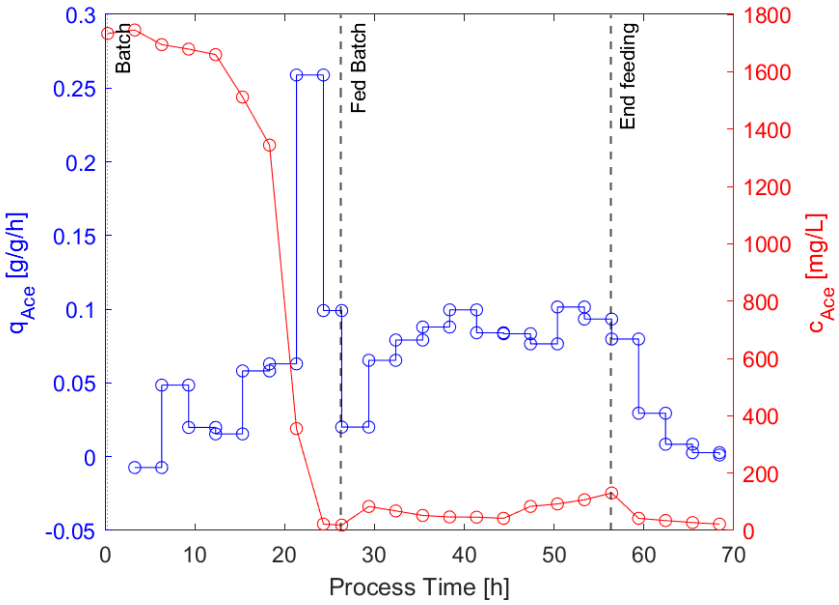

Figure 3.7: Specific acetate uptake rate and acetate concentration over process time.

It is shown in figure 3.8 that the specific pediocin production rate fluctuates into negative values caused by the decrease of the determined titer. These shifting rates and concentrations complicate the identification of the underlying product formation mechanisms as well as model parameter estimation and analysis in a model.

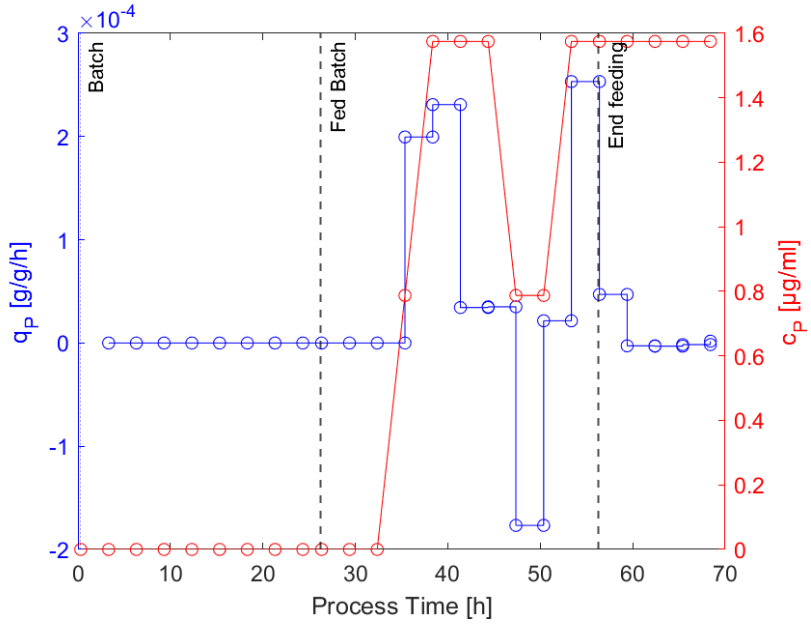

Figure 3.8: Specific pediocin formation rate and pediocin concentration over process time.

3.1.4 Elemental Balance

The conservation law applies to the elemental and electron balances of the bioreactor and is a prerequisite for using the corresponding states of the element in a model. Since this thesis investigates the influence of C, N, and P on the process, the corresponding balances are examined to investigate their applicability to the model. Additionally, the degree of reduction (DoR) was further investigated to determine whether any unknown or unmeasured components of the SSL are oxidized in significant quantities during the process. The ratios of the balances are addressed for the evaluation of reliability, whether they meet the acceptance criterion of 10 %. For the nitrogen balance, 3 different measurements were considered and for the phosphate balance 4. On the other hand, 11 different influencing factors are measured for carbon and DoR. For each measurement, there is a corresponding error rate which complicates successful balancing. The results of the elemental balance calculation are shown in figure 3.9 - 3.12 with an exemplary experiment at the top and boxplot distribution of all the experiments at the bottom. The bar chart corresponds to the measured values of each sample individually whereas the black line represents the sum of the element or electrons provided to the system at the given time. Since the individual sample times of overall performed experiments do not differ significantly, boxplots were calculated over the ratios of all conducted processes for each sample respectively.

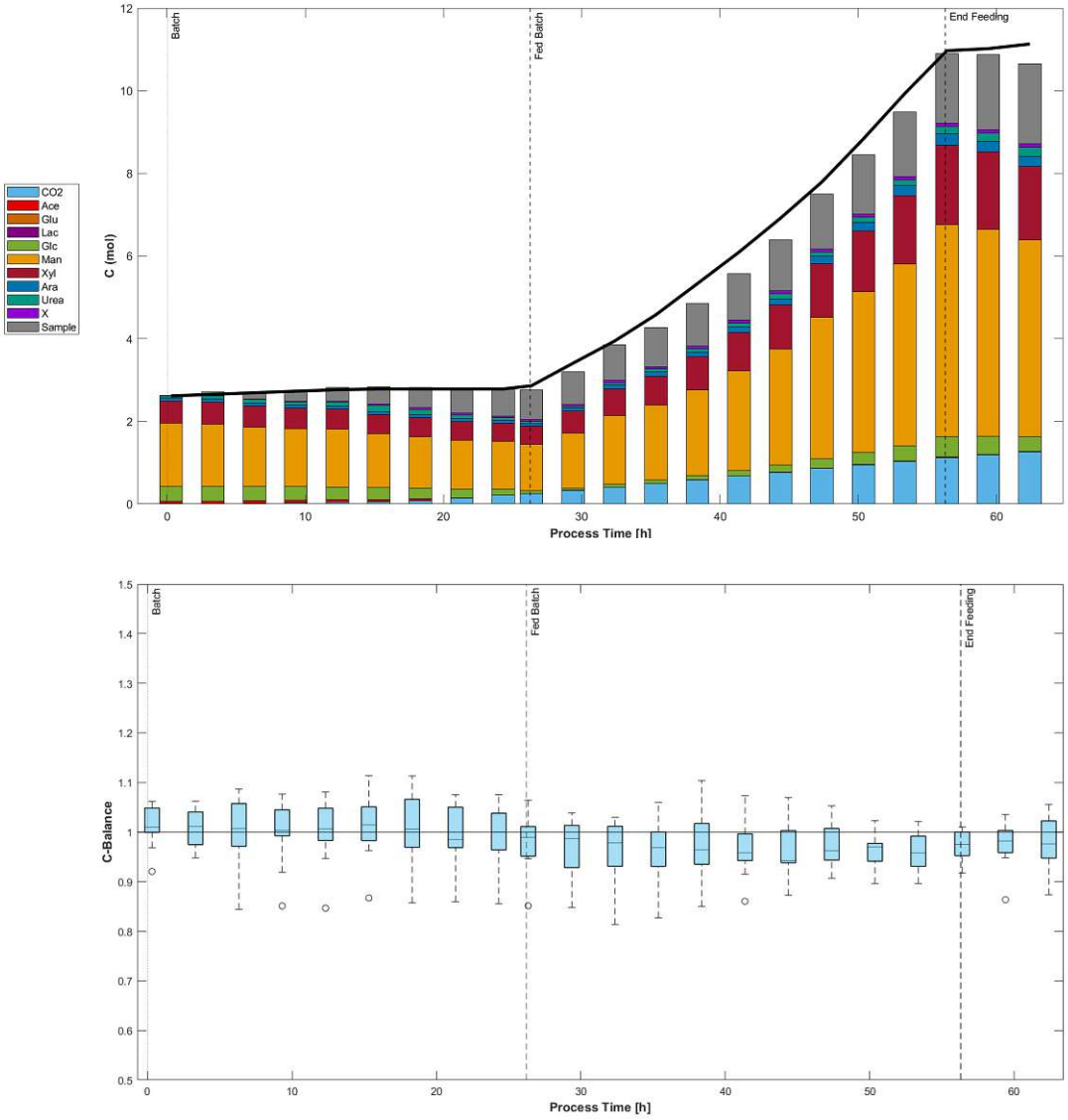

Figure 3.9: Elemental balance of carbon with an example plot of a single experiment (top) and boxplot distribution calculated over all experiments (bottom). The sample points are displayed with their individual, measured composition. The theoretical, total amount over the course of the process is represented as a black line.

It can be seen in figure 3.9, that the total quantity of measured carbon in batch meets the amount supplied to the system, indicating that the carbon can be traced. In the fed-batch phase, the measurements slightly underestimate the provided carbon. The boxplots show that the ratios between the first and third quartiles lie in between the acceptance criterion of ± 10 %, representing 50 % of the ratios of the corresponding samples. Three of the fourth quartiles of the ratios exceed the upper limit of 110 %, indicating an overestimation of the supplied carbon. For the remaining samples, 75 % of the ratios meet the acceptance criterion. Outliers and minimum values are present below 90 % indicating an underestimation of these experiments.

It is shown in the nitrogen balance in figure 3.10 that the element can not be traced throughout the exemplary process. In batch, the measured nitrogen meet the supplied quantities in half of the samples. However, in fed-batch phase, the measured nitrogen differs significantly from the provided nitrogen. Evaluation of overall experiments showed that ammonia concentration is low in samples that deviate significantly from the target value. One reason for this could be the volatilization of ammonia and loss through the exhaust gases[102]. Influence factors of the volatilization are stirrer speed and aeration rates which were controlled adaptively in order to keep the dO value at 30 % in batch and 15 % in fed-batch. The boxplot diagram shows that the ratio between the measurements and the supplied nitrogen deviates successively from the target value of 1 over the process time indicating a systematical error in the measurements of nitrogen. The interquartile range is high during the batch phase with the highest at approximately 16 h process time and levels of to around 20 - 40 % in fed-batch. One reason for the high variance in the batch phase between the processes could be the dynamic behavior of the bacteria at the beginning of the processes. This leads to varying adjustments of stirrer speed and aeration rates, which results in different volatilization of ammonia from experiment to experiment.

The phosphorus balance is displayed in figure 3.11. As described in section 2.6, a non-biomass precipitate is formed in the reaction broth. As a simplification, $Ca_3(PO_4)_2$ was introduced as a secondary compound together with biomass for DCW measurements. The data of the exemplary process show, that with this assumption the samples constantly overestimate the supplied phosphorus throughout the process. This indicates a systematic error in the calculation of the phosphorus balance. In contrast, the balance without precipitation (light gray) as well as lower quantities of removed phosphorus through the samples (dark gray) decreases until the end of the process and not showing a constant error of the calculation. It is shown in the boxplot diagram that phosphorus is significantly overestimated and does not meet the acceptance level. A high interquartile range is seen for the first four samples. Afterwards, the interquartile range is between 140 - 170 %. As the ratios are constantly overestimated and the deviation is low, there is a systematical error in the calculation of the phosphorus balance. One reason for this could be the precipitation of other compounds in addition

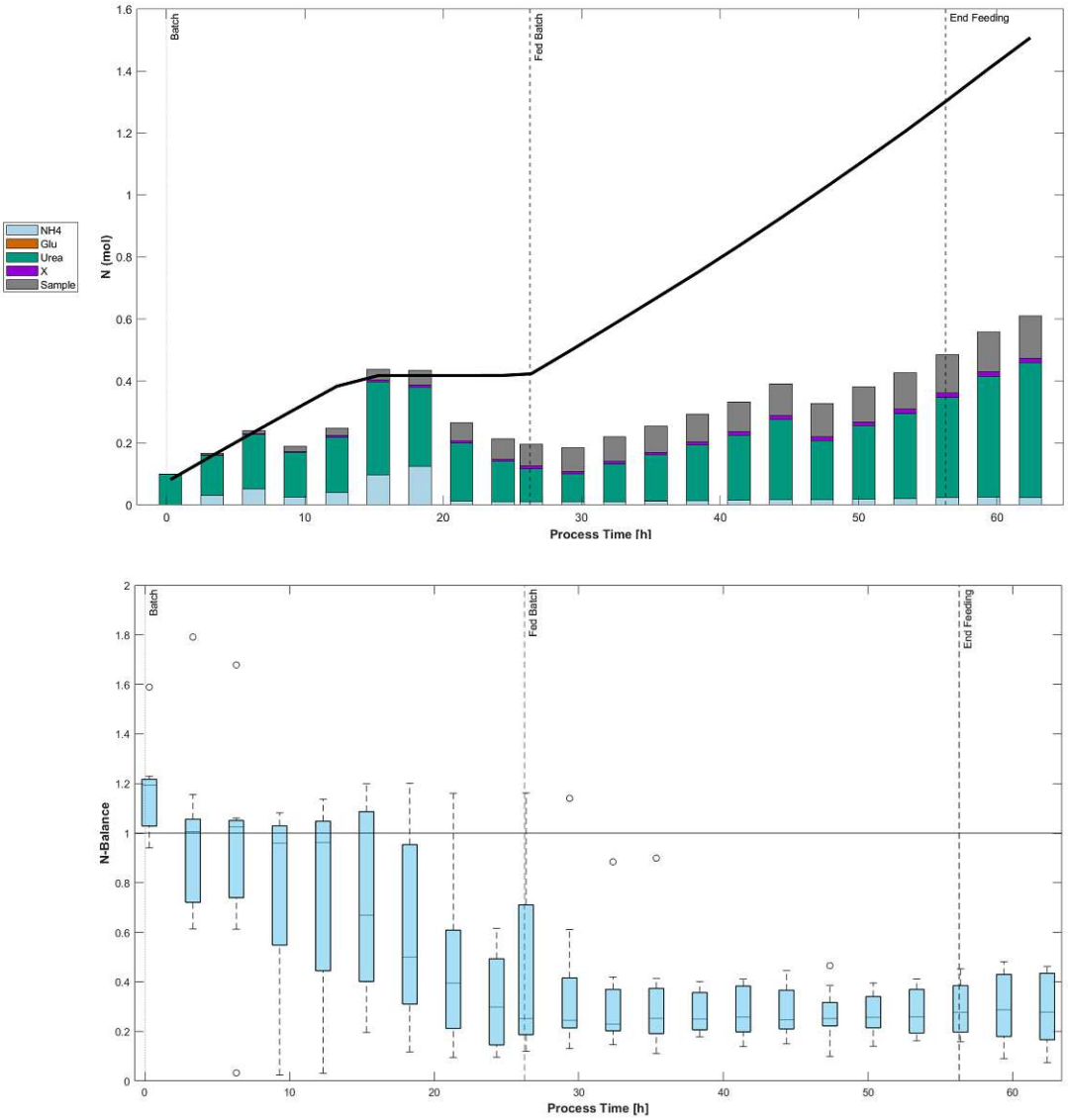

Figure 3.10: Elemental balance of nitrogen with an example plot of a single experiment (top) and boxplot distribution calculated over all experiments (bottom). The sample points are displayed with their individual, measured composition. The theoretical, total amount over the course of the process is represented as a black line.

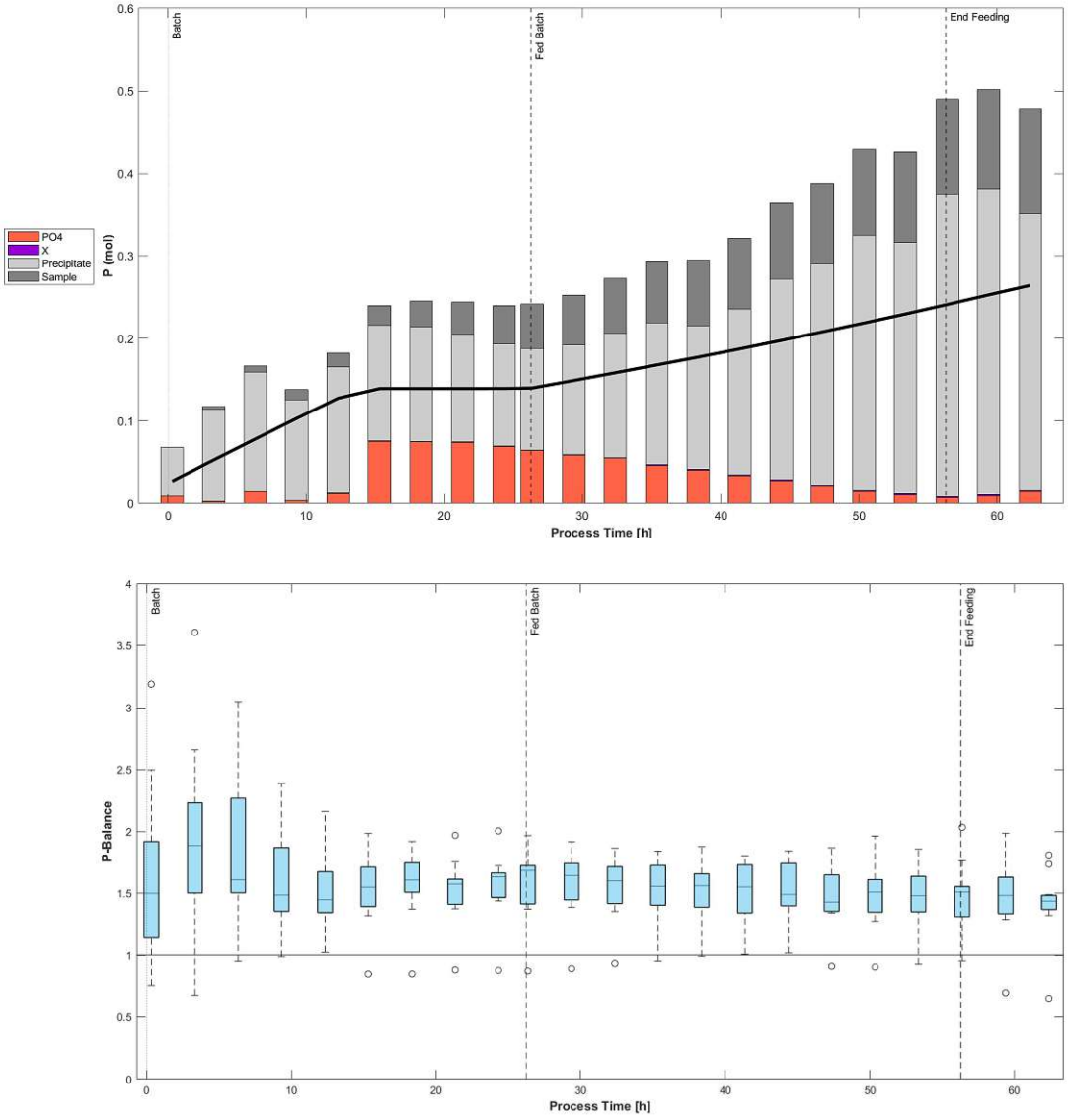

Figure 3.11: Elemental balance of phosphorus with an example plot of a single experiment (top) and boxplot distribution calculated over all experiments (bottom). The sample points are displayed with their individual, measured composition. The theoretical, total amount over the course of the process is represented as a black line.

to $Ca_3(PO_4)_2$, for example, forming of solid Ca_2SO_4 caused by the addition of sulfuric acid for pH control. Further analysis of experimental data showed that a weight content of approximately 50 % of $Ca_3(PO_4)_2$ of the non-biomass DCW would lead to an improvement of the P-balance. In order to check this hypothesis, an elemental analysis of the precipitation should be conducted in order to determine the composition of the precipitate.

It can be seen in figure 3.12, that the results of the DoR-balance are consistent with the results of the C-balance (figure 3.9). The quantities of electrons meet the amount supplied in batch and underestimate it in fed-batch. In the boxplots, the first and third quartiles lie in between ± 10 %. One maximum value exceeds the upper limit, indicating that the remaining 75 % samples fulfill the acceptance criterion. Outliers and minimum values are present below the criterion of 90 %.

The mean of the ratios throughout the single experiments and the corresponding deviations are shown in table 3.1.
The single experiments of the carbon balance meet the acceptance criterion. However, experiment number 4 is at the lower limit with a high deviation, indicating problems with the measurement of the carbon content for this process. For the remaining experiments, the carbon balance lies in the critical acceptance criterion with a deviation of less than 10 %. Therefore, the experimental data which are considered in the C-balance are reliable and can be further used for a model.
For the nitrogen balance, the experiments underestimate the nitrogen content in the samples. The mean values differ significantly from the acceptance criterion with a high deviation. The acceptance criteria can not be met using the existing setup and measurements. Therefore, the data is not reliable with the available measurements and the states can not be included in a model. In order to eliminate the systematic error and to improve the nitrogen balance, an ammonia analyzer could be installed along with the CO_2 and O_2 off-gas analyzers to measure the ammonia loss through the exhaust gases.
The experiments of the P-balance overestimate the phosphorus quantities in the samples significantly, with the exception of experiment 9, where the content is slightly underestimated. Further, the standard deviation ranges from ±10 - 49 % which indicates low robustness of the calculation.
The DoR-balance of the single experiments meets the acceptance criterion. However, the mean ratio of experiment number 4 is below 0.9 with a high deviation which correlates to the outliers in the boxplots. The DoR balance underlines the results of the C-balance and the reliability of the corresponding experimental data. Further, no significant quantities of additional, not-measured compounds are oxidized.

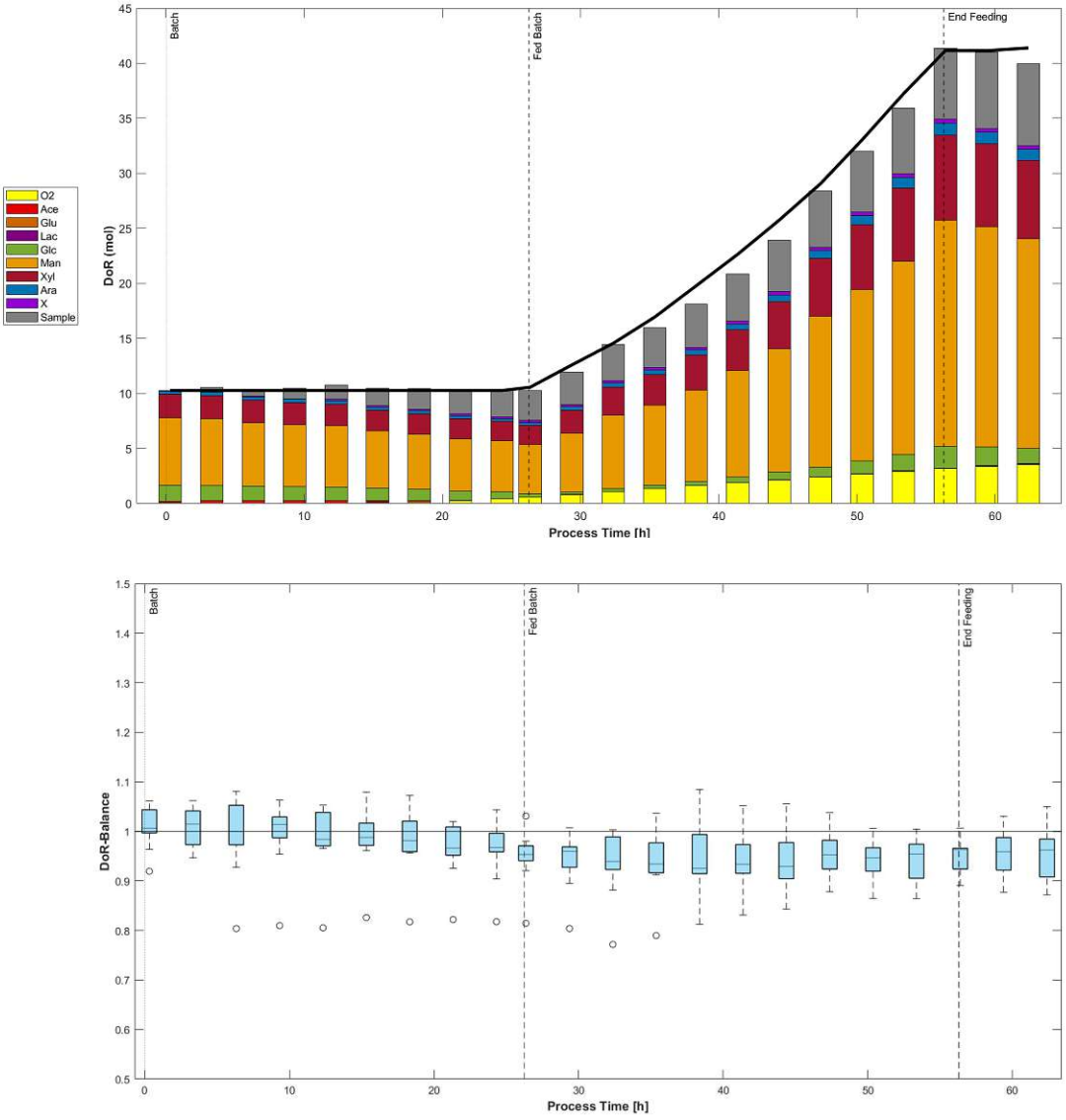

Figure 3.12: Electron balance with an example plot of a single experiment (top) and boxplot distribution calculated over all experiments (bottom). The sample points are displayed with their individual, measured composition. The theoretical, total amount over the course of the process is represented as a black line.

Table 3.1: Mean and deviation of the balance ratios of the individual experiments.

Exp. no	C-Balance	N-Balance	P-Balance	DoR-Balance
1	0.94 ± 0.05	0.53 ± 0.37	1.65 ± 0.26	0.95 ± 0.05
2	1.03 ± 0.03	0.72 ± 0.35	1.47 ± 0.16	1.00 ± 0.03
3	1.01 ± 0.06	0.42 ± 0.41	1.60 ± 0.35	0.96 ± 0.08
4	0.90 ± 0.07	0.48 ± 0.27	1.44 ± 0.14	0.86 ± 0.08
5	1.02 ± 0.04	0.29 ± 0.20	1.39 ± 0.05	0.99 ± 0.04
6	0.97 ± 0.04	0.57 ± 0.28	1.82 ± 0.24	0.97 ± 0.04
7	1.00 ± 0.02	0.49 ± 0.37	1.69 ± 0.16	0.99 ± 0.03
8	0.99 ± 0.05	0.23 ± 0.23	1.38 ± 0.10	0.95 ± 0.06
9	0.96 ± 0.04	0.30 ± 0.22	0.87 ± 0.12	0.96 ± 0.04
10	1.01 ± 0.04	0.56 ± 0.35	1.90 ± 0.31	0.99 ± 0.04
11	0.97 ± 0.02	0.65 ± 0.46	1.87 ± 0.49	0.95 ± 0.02

Summarized, except for experiment 4, the ratios of the C- and DoR-balance fulfill the acceptance criteria of ± 10 %. Therefore, the balances are reliable and the corresponding states can be further used for implementation in the model. Since the inclusion of the experimental data of experiment 4 leads to statistical outliers, it could be considered to repeat the measurements or the whole experiment. The nitrogen balance underestimates the measured nitrogen significantly due to the volatilization of ammonia through the exhaust gases. For the phosphorus balance, the simplification of the DCW with the secondary compound $Ca_3(PO_4)_2$ improves the balance compared to the calculation without this assumption. However, the amount of phosphorus is overestimated constantly, indicating a systematic error. Therefore, an elemental analysis of the precipitation should be conducted. With the current measurements and assumptions, the nitrogen and phosphorus balances do not meet the acceptance criterion and the experimental data is therefore insufficient to be implemented in a model.

3.1.5 Design of Experiment

The values of the different experiments for the DoE are shown in figure 3.2. The mean of the specific growth rate and pediocin concentration were used as response values for growth and product titer. Additionally, the first sample of the fed-batch was excluded from the calculation in order to avoid possible effects of the uninduced phase, for example, the specific growth rates of the beginning of the fed-batch are higher compared to the remaining fed-batch. For the response value biomass growth, different setups (mean/max; biomass concentration/specific growth rates) have been tested. For the pediocin titer, the values are on fixed levels with a corresponding high error range due to the nature of the pediocin assay (Section 2.7). Therefore, the mean value of the titer was used for the DoE in order to compensate for a possibly too-high measured maximum concentration.

Table 3.2: Factors and Response of DoE.

Run Order	SSL [%]	n_C/n_N	n_C/n_P	$\overline{\mu}$ $[\frac{g_X}{g_X h}]$	$\overline{c_P}$ $[\frac{\mu g}{mL}]$
1	50	5	45	0.015	1.18
2	37.5	7.5	30	0.012	0.04
3	25	10	45	0.014	2.09
4	25	5	15	0.001	0.12
5	25	5	45	0.011	0.54
6	37.5	7.5	30	0.018	0.00
7	50	10	15	0.009	0.00
8	50	5	15	0.018	0.19
9	25	10	15	0.014	0.50
10	37.5	7.5	30	0.015	0.06
11	50	10	45	0.019	0.64

For the response value growth, no significant model term was found by the DoE. However, for the response value pediocin concentration, the DoE indicates a significant impact of the applied phosphate concentration of the NP feed in the fed-batch. The model statistics, summary of fit (SoF) and analysis of variance (ANOVA), of the response values are shown in table 3.3.

As the model fit (R2) of the response value growth is below 0.5, the model has a low significance, indicating that the independent variables do not correlate with the dependent variable. Predictability (Q2) measures the predictive power of the model. A value below 0.10 indicates that the model is not significant. Model validity indicates that the model is appropriate and that there are no significant model problems, for

example, outliers, transformation problems or an incorrect model. The reproducibility bar reflects the variation of the replicates and has to be above 0.5 for a good model. The upper F-test evaluates the regression model if it fits the data as well as a model without the independent variables. The probability value (p-value) of 0.15 does not meet the significance level of 0.05, indicating that the independent variables are not statistically significant for the response value growth. The p-value of lack of fit is above the significance level of 0.05, which indicates that the variation between the actual data and the fitted model is not significant. Since no significant model terms were found for the response value growth, further evaluation plots are not shown.

For the response value pediocin titer, a quadratic model term was included as it resulted in a significant improvement of the model (figure 3.13). The DoE would have to be expanded to a face-centered DoE for validation of this assumption. However, this hypothesis is examined in the model in which the product formation is described. An R2 of 0.76 indicates that the independent variables correlate with the pediocin concentration. Q2 has a value above 0.5 which reflects a good model and the model validity shows that there are no significant model problems. Additionally, the reproducibility of 0.95 indicates a good model. The p-value of the regression of 0.003 is below the significance level of 0.05, indicating that the applied model provides a better fit to the data than a model without the independent variables. For lack of fit, a p-value of 0.117 was determined which is greater than the significance level of 0.05.

Table 3.3: DoE model statistics

		$\overline{\mu}$	$\overline{c_P}$	Reliable model
Summary of fit				
	R2	0.21	0.76	> 0.50
	Q2	0.05	0.66	> 0.10
	Model validity	0.61	0.46	> 0.25
	Reproducibility	0.74	0.95	> 0.50
ANOVA				
	p-value (Regression)	0.15	0.003	< 0.05
	p-value (Lack of fit)	0.21	0.117	> 0.05

For the response value pediocin concentration, the DoE indicates a significant impact of the model terms 1/P and 1/P*1/P on the product titer (figure 3.13). The quadratic term is larger than the non-square term indicating a higher significance. The lower the applied phosphate concentration of the NP feed in the fed-batch, the higher the pediocin titer in the reaction broth within the value range of n_C/n_P of 1:15 - 1:45.

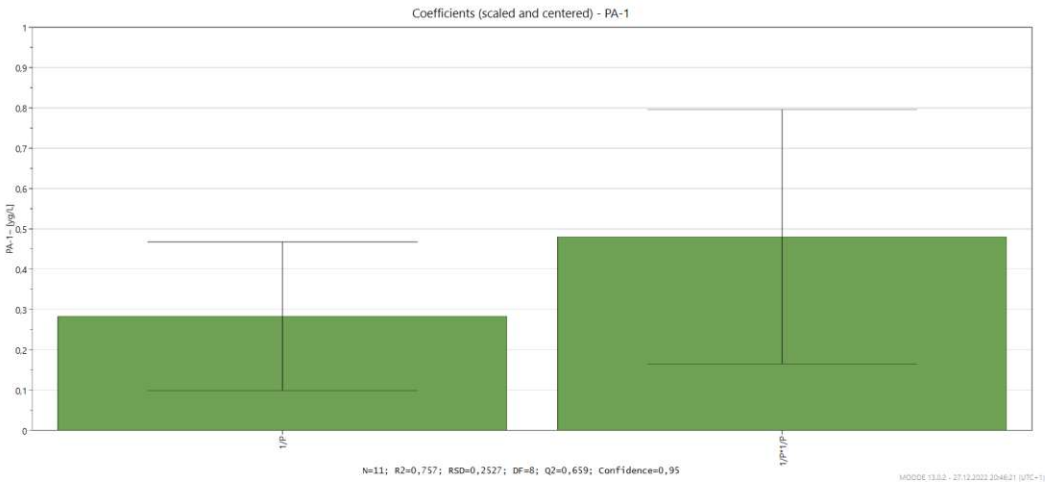

Figure 3.13: The coefficient plot of the response value pediocin shows a significant impact of the model terms 1/P and 1/P*1/P on the product titer.

The replicate plot (figure 3.15) shows that the replicates have a small variability compared to the overall variability of the experiments, indicating that they do not deviate significantly from each other.

The residual normal probability plot (figure 3.14) displays if the residuals of the obtained data are normally distributed noise. The ideal outcome is that the experiments are on a straight line and points outside should be checked for outliers. Experiments 6 and 9 deviate from the remaining experiments. However, the model validity is above 0.25 and the p-value of the lack of fit is above the significance level of 0.05 (table 3.3), indicating that there are no outliers or other significant model problems.

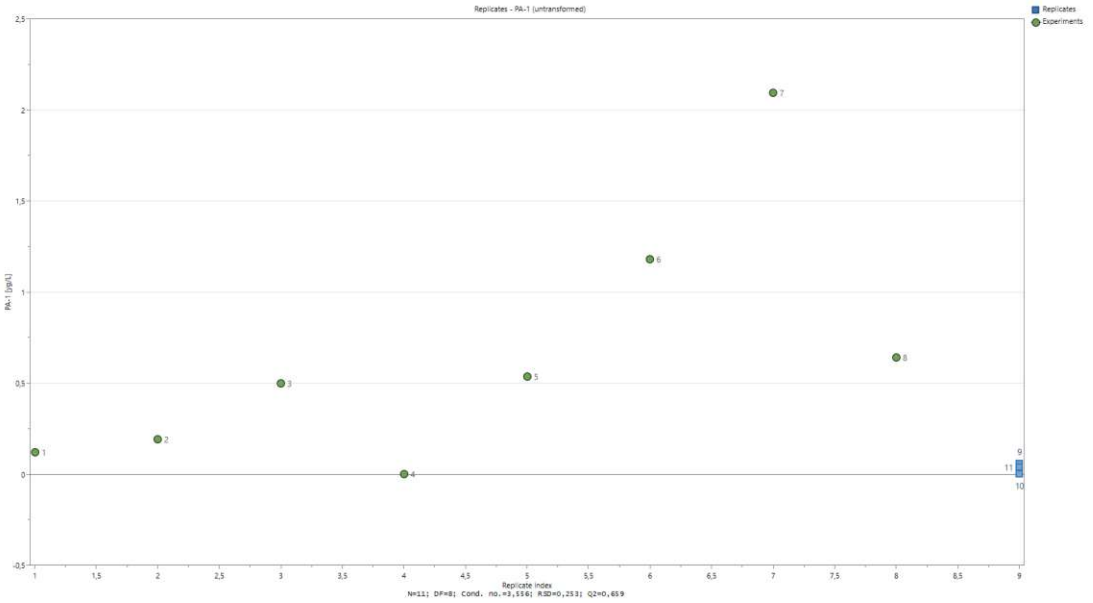

Figure 3.14: The replicates have a small variability compared to the overall variability. The replicates do not significantly deviate from each other.

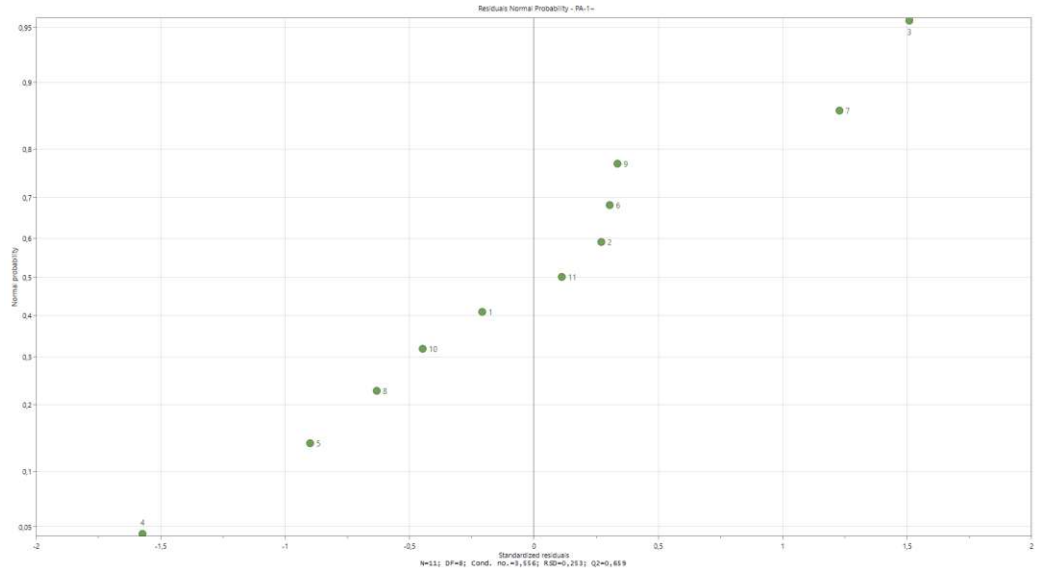

Figure 3.15: The residual plot of the response value pediocin titer indicates that experiments 6 and 9 could be outliers.

The contour plot of the predicted response values (figure 3.16) shows the influence of the factor n_C/n_P on the product titer. The maximum is located at 1/45 at the edge of the factor range, indicating that the optimum of the pediocin production was not covered by the boundaries. Therefore, the DoE should be shifted toward higher phosphate limitation in order to investigate the optimal conditions for pediocin production. The applied levels of SSL and nitrogen have no impact on the product titer, indicating that the applied quantities are sufficient for product formation. However, lower quantities of the precursors with consistent pediocin rates would increase economic viability in industrial production, making an examination of lower concentrations of the factors attractive for further investigations.

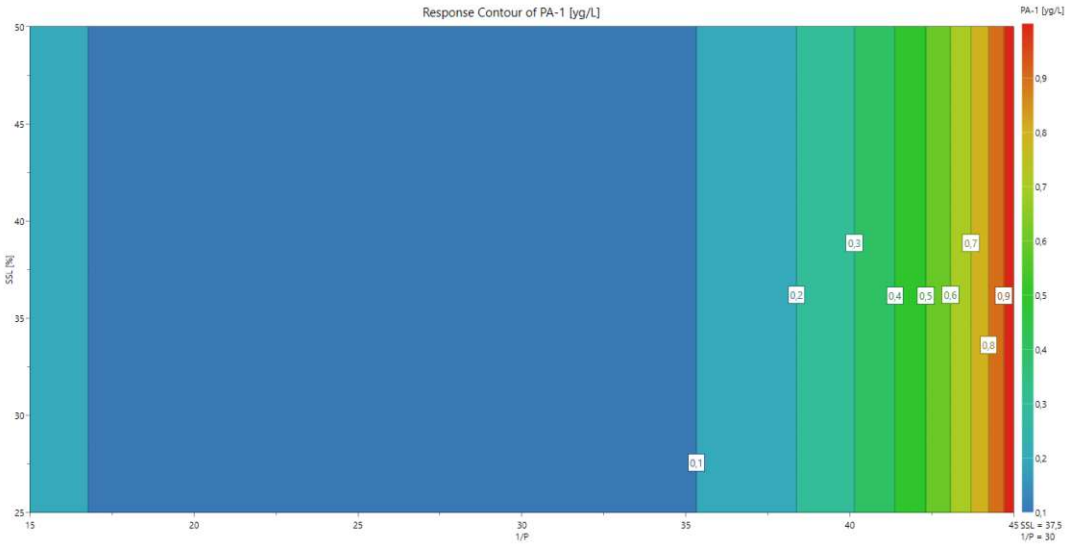

Figure 3.16: The contour plot shows that the highest product titers are observed with n_C/n_P of 1:45. This maximum concentration is located at the edge of the DoE, which indicates that the optimum of the factor on the titer is not covered by the boundaries of the DoE.

Summarized, the factors of the DoE have no significant effect on the growth in the fed-batch. Growth rates are substantially reduced in the induced phase compared to the batch phase (Section 3.1.3). Consequently, optimizing the overall growth rates in fed-batch has a minor impact on the biomass concentration. Therefore, the batch conditions should be further investigated in order to increase the starting biomass in fed-batch or to increase the space-time yield by reducing the duration of the batch. However, an uninduced fed-batch with a feed ramp of μ_{max} would be another alternative in order to increase the biomass. The factor n_C/n_P has a significant influence

on the pediocin formation and therefore, the phosphate concentration state should be implemented in the pediocin formation mechanistics of the model. Since the P-balance does not meet the required acceptance criteria (section 3.1.4), this state must not be adopted. However, a simplification can be met by using the factor n_C/n_P as a constant over the fed-batch time and neglecting the mechanistics of phosphate uptake as well as precipitation formation.

3.2 Model Evaluation

The mechanistic model used in this study was based on the model described in [56] and adapted to the performed experiments. As discussed in section 3.1.3, the physiological properties of the bacterium change in the induced fed-batch. In order to simplify the model structure, batch and fed-batch were analyzed separately. The experimental data was split and two different model parameter sets were fitted by the algorithm as well as analyzed for overall model fit. The batches were executed with identical conditions and should therefore show a similar progression in contrast to the fed-batches, in which varying feeding concentrations were applied. As a simplification, the C-sources were designated with S_1 - S_4 (glucose, mannose, xylose and acetate) the biomass with X and pediocin with P to enhance readability.

Specific Rates and Growth Kinetics

The specific substrate uptake rates of glucose, mannose, xylose and acetate (q_i) are shown in equation 3.1 - 3.4. The uptake rates were implemented using Monod kinetics with the substrate concentration (S_i), the half-velocity constant (K_i) and the maximum specific uptake rate ($q_{i,max}$). For mannose and xylose, a mixed inhibition term of the respective other sugar and glucose was introduced. An inhibition phase of the acetate uptake occurred in all conducted experiments. Therefore, a term for the inhibition phase was included according to [103]. The inhibition term t_{Inh} was determined by a drop of the dO signal of 3 % from the maximum value.

$$q_{S1} = q_{S_1,max} \cdot \frac{S_1}{S_1 + K_1} \tag{3.1}$$

$$q_{S2} = q_{S_2,max} \cdot \frac{S_2}{S_2 + \frac{K_{S2}}{K_{S1}} S_1 + \frac{K_{S2}}{K_{S3}} S_3 + K_{S2}} \tag{3.2}$$

$$q_{S3} = q_{S_3,max} \cdot \frac{S_3}{S_3 + \frac{K_{S3}}{K_{S1}} S_1 + \frac{K_{S3}}{K_{S2}} S_2 + K_{S3}} \tag{3.3}$$

$$q_{S4} = q_{S_4,max} \cdot \frac{S_4}{S_4 + K_4} \cdot \left(1 - e^{-\frac{t}{t_{Inh}}}\right) \tag{3.4}$$

The Biomass growth (equation 3.5) is a combination of the individual sugar uptake rates and the respective yields (Y_{X/S_i}).

$$\mu = q_{S1} \cdot Y_{X/S1} + q_{S2} \cdot Y_{X/S2} + q_{S3} \cdot Y_{X/S3} + q_{S4} \cdot Y_{X/S4} \tag{3.5}$$

The pediocin formation was described with a substrate inhibition kinetics. It is calculated with an induction term to differentiate between induced and non-induced phase, the maximum product formation rate ($q_{P,max}$), the carbon to phosphate ratio (n_C/n_P) and the maximum molar phosphate to carbon ratio ($n_{C/P,max}$).

$$q_P = Induction \cdot q_{Pmax} \cdot \left(1 - \frac{n_{C/P,max}}{n_C/n_P}\right) \cdot \left(1 - \frac{n_{C/P,max}}{n_C/n_P}\right)^2 \tag{3.6}$$

Differential equations

The differential equations of a fed-batch mode in an ideal stirrered tank reactor are shown in equation 3.7 - 3.10. These functions describe the changes of the reactor volume (V_R) and the concentration of the biomass (X), the substrates (S_i) and the product (P) over time with the substrate inflow $\dot{V}_{in}$, the dilution rate D and the corresponding reaction rates. In order to account for the product inactivation due to the oxygen sensitivity of pediocin [88], an oxidation rate term (q_{dO}) was included. In batch, $\dot{V}_{in}$ is 0 and D is influenced by the inflow of acid and base.

$$\frac{dV_R}{dt} = \dot{V}_{in} \tag{3.7}$$

$$\frac{dX}{dt} = X \cdot (\mu + D) \tag{3.8}$$

$$\frac{dc_{S_i}}{dt} = \frac{\dot{V}_{S_i,in}}{V_R} \cdot c_{S_i,in} - D \cdot c_{S_i} + q_S \cdot X \tag{3.9}$$

$$\frac{dc_P}{dt} = -c_P \cdot (D + q_{dO}) + q_P \cdot X \tag{3.10}$$

Model Parameters

The model parameters were estimated with an algorithm minimizing the negative log likelihood (section 2.7) and the fitted parameters of batch and fed-batch are shown in table 3.4. The model parameters of batch and fed-batch differ from each other. The maximum substrate uptake rates of glucose and acetate are higher compared to batch. In contrast the uptake rates of mannose and xylose are lower. In fed-batch the

biomass yields of the individual sugars are significantly lower than in batch, due to the increased metabolic burden by the product formation.

Table 3.4: Model parameters of batch

	Parameter	Batch	Fed-batch	Unit
Substrate Uptake Rates				
	$q_{S1,max}$	0.265	0.389	g g^{-1} h^{-1}
	$q_{S2,max}$	0.248	0.122	g g^{-1} h^{-1}
	$q_{S3,max}$	0.154	0.082	g g^{-1} h^{-1}
	$q_{S4,max}$	0.101	0.281	g g^{-1} h^{-1}
Yields				
	$Y_{X/S1}$	0.250	0.058	g g^{-1}
	$Y_{X/S2}$	0.204	0.141	g g^{-1}
	$Y_{X/S3}$	0.225	0.071	g g^{-1}
	$Y_{X/S4}$	0.038	0.006	g g^{-1}
Half Velocity Constants				
	K_{S1}	0.005	0.075	g L^{-1}
	K_{S2}	0.528	0.697	g L^{-1}
	K_{S3}	1.774	0.717	g L^{-1}
	K_{S4}	0.001	0.216	g L^{-1}
Product specific Parameters				
	$q_{P,max}$	-	2.800	μg g^{-1} h^{-1}
	$c_{PO_4,max}$	-	0.035	Pmol $Cmol^{-1}$
	q_{dO}	-	0.080	μg μg^{-1} h^{-1}

Model fit - Batch

The results of the time-resolved states (biomass, glucose, mannose, xylose and acetate) of the exemplary process are shown in figure 3.17.
The model accurately predicts the biomass concentrations (top left) in the early stages of the process with a deviation of 0.06 g L^{-1} until approximately 10 h process time. Afterwards, the increase of the biomass is not valued by the model, resulting in an underestimation of 0.33 g L^{-1} on average for the samples 5 - 8. However, in the last sample, the estimated concentration meets the experimental data.
For the state glucose (top right), the course of the concentration is accurately predicted with a deviation of approximately 1.1 g L^{-1}. The decrease of the concentrations of the sugars mannose (middle left) and xylose (middle right) is accurately predicted with a deviation of about 0.92 g L^{-1} by the model.

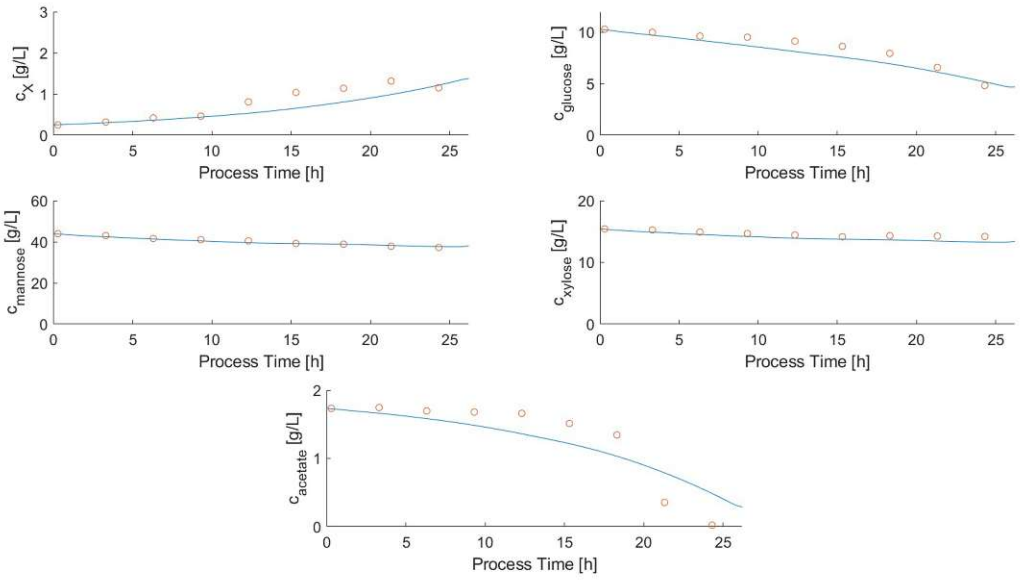

Figure 3.17: The measured values (circles) and the predicted values (blue line) of the time-resolved state´s biomass and glucose (top), mannose and xylose (middle) and acetate (bottom) of an exemplary process in batch.

For acetate (bottom), the model predicts an uptake over a longer time period compared to the experimental data. One reason for this is a stronger inhibition of the uptake of the organic acid, resulting in the onset of the uptake at a later point in the process compared to the model description. The specific uptake rate is higher leading to faster consumption of acetate. However, in this time-area only a few measurement points

are given. Furthermore, as the measurement procedure in CEDEX is not designed to measure samples with SSL background, the method could give falsified results at a lower concentration area. In order to check this hypothesis, SSL from the end of the fermentation could be separated from the cell mass and spiked with different acetate concentrations. Acetate measurements could subsequently rule out the influence of an SSL background. However, due to limited time, these experiments were not performed.

The observed vs. predicted plots of the batch are displayed in figure 3.18. Every batch was executed with identical conditions. However, the starting biomass concentrations as well as the inhibitor- and sugar concentrations in the SSL deviate from experiment to experiment. In addition to biological variability, divergent behavior of the individual experiments is expected leading to scattering in the observed vs. predicted plots.

At around 0.23 - 0.6 g L^{-1}, the biomass concentration (top left) is accurately predicted. With higher biomass, an increased scattering is observed with an underestimation of most of the samples. However, some samples between approximately 0.6 - 1.6 g L^{-1} are overpredicted by the model leading to difficulties fitting the model data to the experimental data by the algorithm. This indicates that the model can not predict the variability in the results based on the slightly different inputs at the start of the batch.
For the state glucose (top middle), the model underestimates the concentration between 4 - 10 g L^{-1} leading to a high scattering in the observed vs. predicted plot. In the lower concentration areas, the model underestimates the uptake of the sugar for some experiments. However, for these experiments, the biomass concentration is underpredicted by the model. For example in experiment 4, the concentration is underpredicted in the concentration area of approximately 1.1 - 2.6 g L^{-1}. As the biomass concentration has a major impact on the total uptake of the substrates, inaccuracies in the prediction influence the other states significantly. For mannose (top right) and xylose (bottom left), the model can accurately describe the uptake of the sugars with a deviation of approximately 0.78 and 0.36 g L^{-1} on average.
For the observed vs. predicted plot of acetate (bottom right), two areas are seen: Between approximately 1 and 1.7 - g L^{-1}, the uptake of the organic acid is overpredicted by the model except for 3 experiments. However, at 0 - 0.1 g L^{-1}, the model overestimates the concentration in the samples. One reason for this could be that the method has problems at low concentrations by hitting a limit of detection (LoD), which is indicated by only 5 measurement points in between 0.1 - 0.9 g L^{-1}. In contrast, the organic acid uptake could be high, resulting in few samples in this range. Therefore, as a next step, the LoD should be tested as described in the discussion of the time-resolved states of the batch or the sample time could be substantially reduced in the area of the uptake.

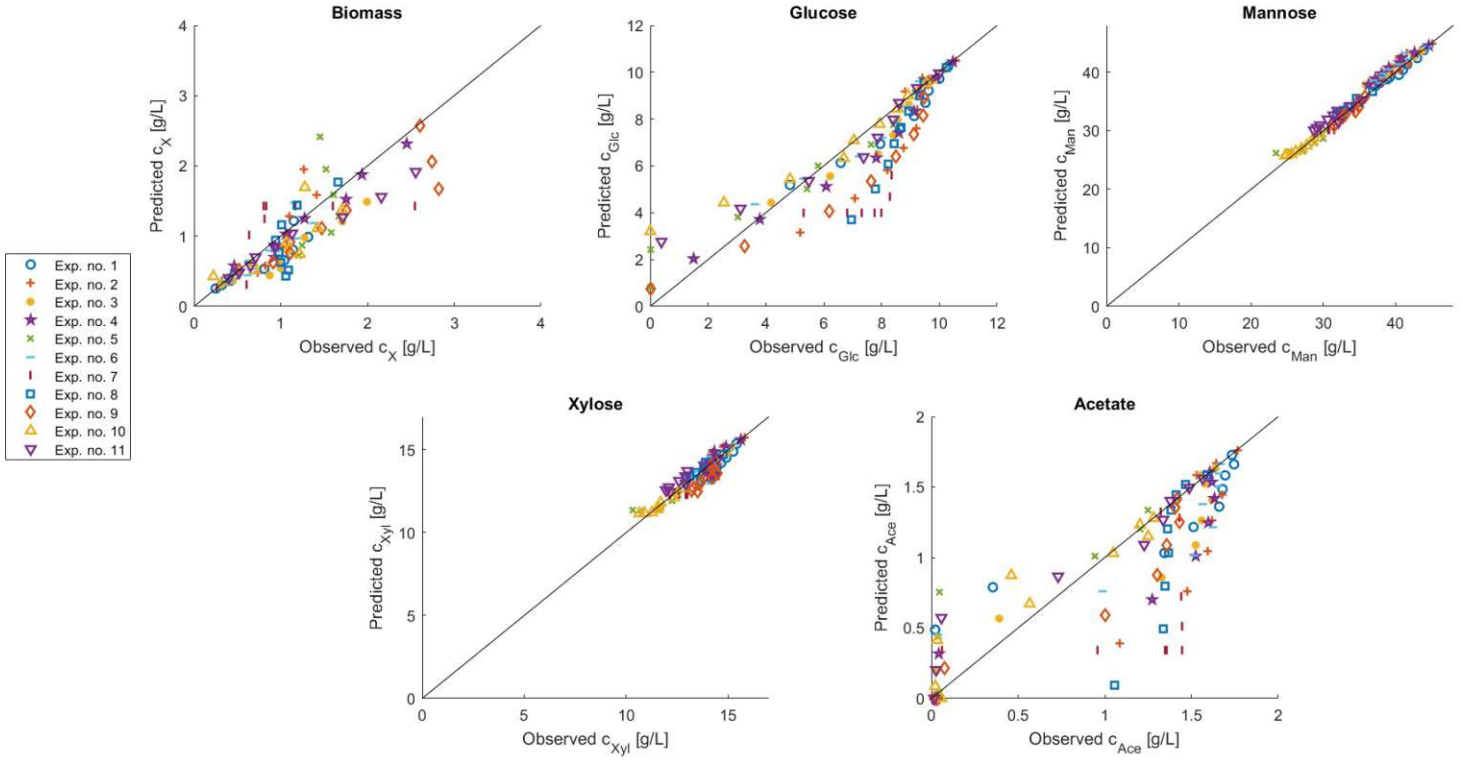

Figure 3.18: The predicted values on the y-axis plotted against the observed values on the x-axis for all performed samples during the batch of all experiments. The observed values are on the x-axis and the predicted ones on the y-axis. A perfect prediction is reflected by the x = y line.

The NRMSE values with the corresponding standard deviations of the states biomass, glucose, mannose, xylose and acetate in batch are shown in table 3.5. The error rate of biomass is at approximately 30 % with a standard deviation of 10 %. One reason for this is the high variability of the initial biomass, caused by the low concentration area and the high error range of the measurement. Furthermore, biomass prediction inaccuracies have a large impact on the other states. In order to improve the overall prediction power of the model, the error margin of the measurement could be reduced or the starting biomass increased.
For the state glucose, the NRMSE is at 16.60 % with a deviation of 8.4 % which is above the acceptance criterion of 15 %. As stated in the discussion of the observed vs. predicted plots, the inaccuracies of the biomass prediction influence the glucose significantly.
As the error rates of mannose (2.68 %) and xylose (3.28 %) meet the acceptance criterion of 15 %, these states can be accurately predicted by the model. Furthermore, the standard deviation is at approximately 1 %, indicating that the model has a high prediction quality and robustness for the prediction.
For acetate, the error rate is at approximately 32 % with a standard deviation of 13 %, indicating problems of the model predicting this state or measurement problems.

Table 3.5: NRMSE and the corresponding standard deviation of the states biomass, glucose, mannose, xylose, acetate and in batch.

	Biomass	Glucose	Mannose	Xylose	Acetate
NRMSE (in %)	29.99	16.60	2.68	3.28	31.83
StDev of NRMSE	10.01	8.41	0.92	1.01	13.09

Summarized, the model can accurately predict the sugars mannose and xylose in the batch phase. However, the model fails for predicting the state biomass in the higher concentration area. Further, the prediction of the biomass concentration has a major impact on the glucose prediction with an NRMSE of 16.60 % which is above the acceptance criterion. For the organic acid acetate, measurement errors may be present in lower concentration ranges which complicates the modeling of this state.

Model fit - Fed-batch

The time-resolved states of the exemplary process during the fed-batch are shown in figure 3.19.

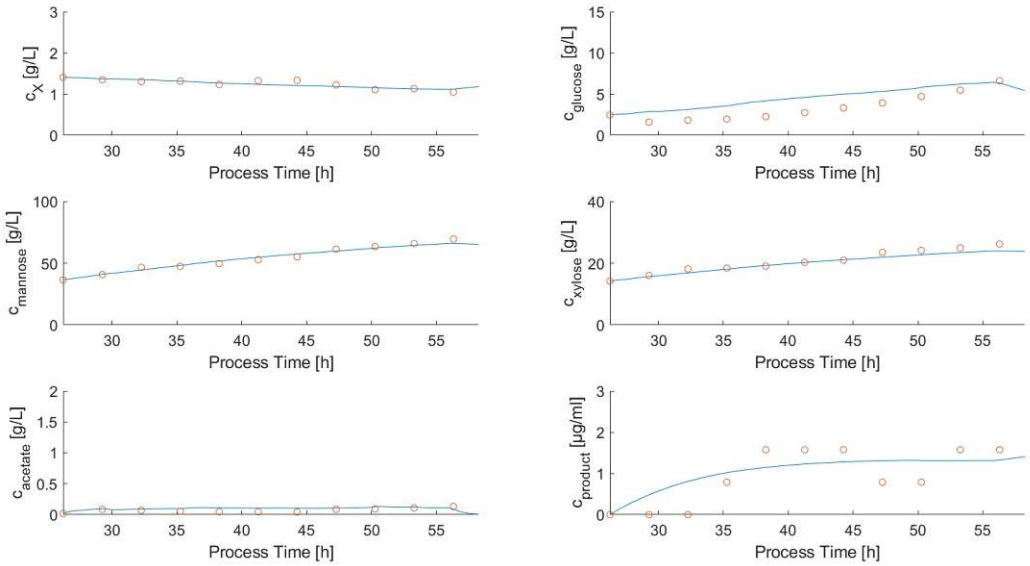

Figure 3.19: The measured values (circles) and the predicted values (blue line) of the time-resolved state´s biomass and glucose (top), mannose and xylose (middle) as well as acetate and pediocin (bottom) of an exemplary process in fed-batch.

Cell growth is low in the induced phase and the dilution of the biomass concentration (top left) is accurately predicted by the model with a deviation of 0.07 g L^{-1} on average. For the state glucose (top right), the sugar has not been fully utilized in the batch phase as seen in sample 1. The model underestimates the uptake throughout the process but meets the concentration in the end of the fed-batch. For the sugars mannose (middle left) and xylose (middle right), the model can accurately predict the concentrations with a deviation of 1.62 g L^{-1} and 0.81 g L^{-1} on average.
For the state acetate (bottom left), the measured concentrations are at low levels at approximately 0 - 0.2 g L^{-1} which is accurately predicted by the model with a deviation of approximately 0.03 g L^{-1} on average.
As seen for pediocin (bottom right), the concentration increases in the beginning of fed-batch. Afterwards, the titer remains stable between 0.8 - 1.6 μg ml^{-1}. One reason for this could be that the induction effects are diminishing in the later stages of the process which could be caused by a decrease of the IPTG concentration in the reaction

broth or habituation of the cells to IPTG. The model estimates an earlier formation of the product in the exemplary process. The operon *pedACD* encodes for the precursor of pediocin and proteins which are responsible for processing, cleavage and segregation (Section 2.1). The time from the start of the induction over to the accumulation of the protein in the reaction broth, therefore, causes a shift of the later measured increase to the simulation data. In order to represent this delayed accumulation in the model, an inhibition term could be integrated into the specific rate, similar to acetate. After approximately 35 h process time, the predicted pediocin concentration is within the error range of the measurement.

The observed vs. predicted plots of the fed-batch are shown in figure 3.20. The biomass content of the samples (top left) scatters within the measurement error of 0.17 g L^{-1}, reflecting an accurate prediction by the model.
Low glucose concentrations (top middle) can be accurately predicted by the model as well as higher concentrations of process 2. However, higher measured glucose concentrations are either over- or underpredicted, resulting in a high scattering. These experiments correlate to SSL concentrations of 37.5 % or 50 %, indicating problems of the model prediction with the higher boundaries of the factor.
For mannose (top right) and xylose (bottom left), the measured values can be accuratly predicted by the model within a scattering range. For experiment 6, the model underpredicts the concentrations significantly. Further, for xylose, one process is significantly overestimated and deviate from the target value, the 45° line.
With the exception of 3 samples, the acetate measurement values (bottom middle) are within concentrations of less than 150 mg L^{-1}. These low concentrations have only a minor effect on growth or the prediction of the other states lowering the importance of the state on the overall model prediction.
For pediocin (bottom right), the two-fold dilution series detection method of the assay is seen as a doubling of the concentrations within an experiment. Two different standard concentrations were used for the determination of the pediocin concentration. Therefore, two different concentration profiles are seen in the observed vs. predicted plot. The order of the samples within an experiment with formed pediocin can be assessed by a successive increase in the predicted value. For example in experiment 3, the last measured values are at approximately 3.2 μg mL^{-1}. A high scattering is observed in the plot with an under- and overestimation of the pediocin concentration. The step formation of the determined titers as well as the high error rate of the measurements complicates the modeling of the state and identification of the product formation mechanisms of the bacteria.

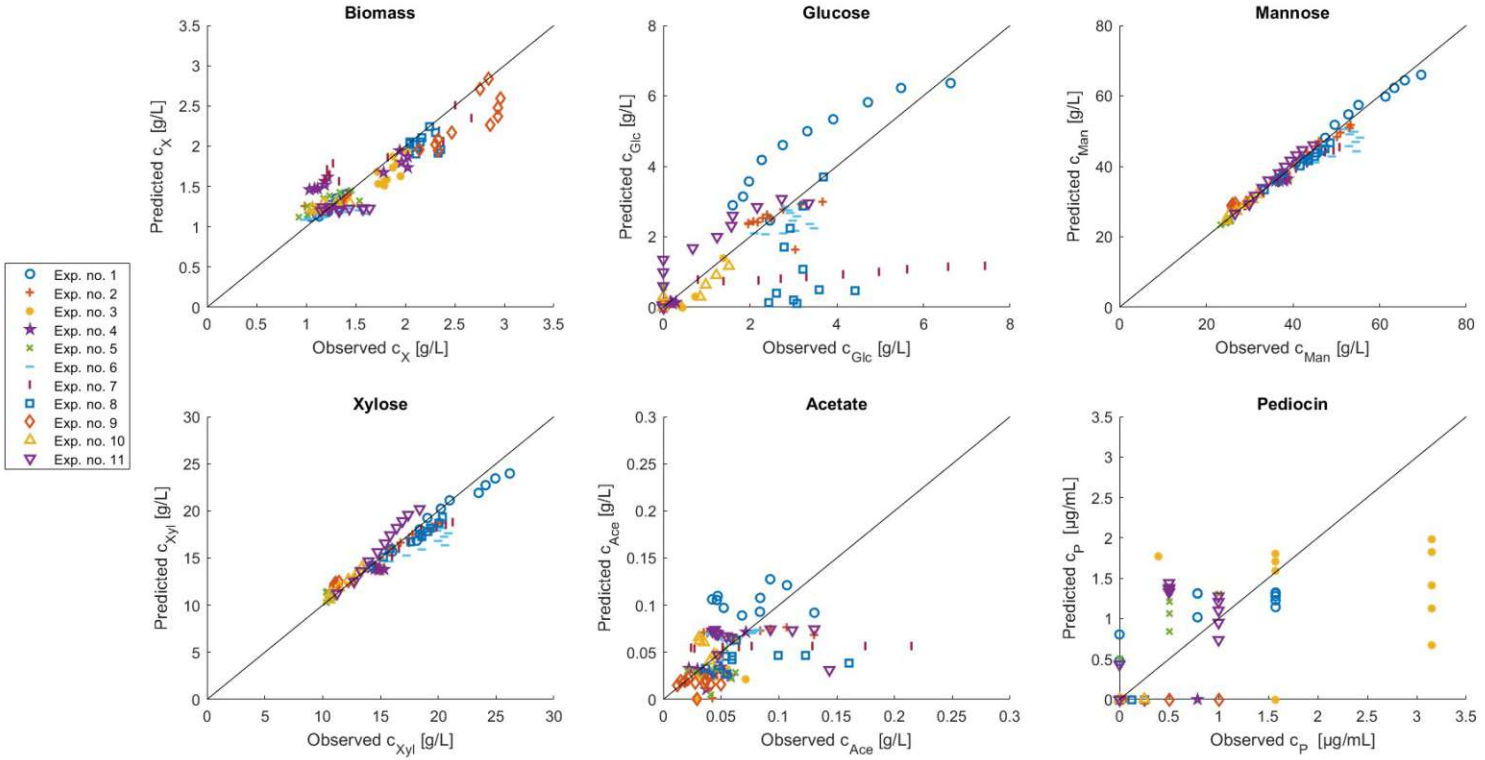

Figure 3.20: The predicted values plotted against the observed values for all performed samples of all experiments in fed-batch. The observed values are on the x-axis and the predicted ones on the y-axis. A perfect prediction is reflected by the x = y line.

The NRMSE values with the corresponding standard deviations of the states biomass, glucose, mannose, xylose, acetate and pediocin in fed-batch are shown in table 3.6.
The state biomass meets the acceptance criterion of less than 15 % which indicates an accurate prediction. Further, the standard deviation 4.80 % is low, reflecting a good robustness.
For glucose, the error rate is at approximately 57 ± 26 %, which reflects a low prediction quality and reproducibility of the model for this state. In contrast, the NRMSE values of 4.78 and 6.89 % of the sugars mannose and xylose meet the acceptance criterion. Additionally, the low standard deviation indicates a high reproducibility of the model for this states.
For acetate, the NRMSE is at approximately 56 %. However, the NRMSE does not reflect the importance of the state on the model and the other states. As seen in the observed vs. predicted plots, the values are in a low concentration area. This results in a high calculated NRMSE due to dividing by the mean value (Section 2.7). In contrast, the RMSE is at approximately 32.8 mg $L^{-}1$ for the given data.
The high error of the pediocin prediction is caused by the inaccuracy of the assay. Therefore, no assessment of the prediction performance can be concluded.

Table 3.6: NRMSE and the corresponding standard deviation of the states biomass, glucose, mannose, xylose, acetate and pediocin in fed-batch.

	Biomass	Glucose	Mannose	Xylose	Acetate	Pediocin
NRMSE (in %)	12.54	57.38	4.78	6.89	55.79	98.18
StDev of NRMSE	4.80	25.61	2.94	3.76	20.84	69.32

Summarized, the model can accurately predict biomass growth and the sugars mannose and xylose in fed-batch. However, the model fails to predict the states glucose and acetate, whereby acetate has only a minor impact on the overall model prediction due to the low concentration area. For the state pediocin, the model can predict the titers within the error range. The measurement assay does not provide values with a high precision which hinders an assessment of the prediction quality.

3.3 Comparison to Literature

Current process and model developments of *C. glutamicum* were based on complex media with an addition of 5 - 10 % SSL as a carbon source [53, 56, 57, 58]. However, it could be shown that processes based on pure SSL without the addition of complex media or other additives can be carried out. This enhances the economics and reduces the operational effort of future industrial bioprocesses utilizing the waste stream media.

Balancing is an important tool to assess the consistency and reliability of the data or to reveal non-accounted components which are present in significant quantities [25]. However, as far as known, this elemental approach has not been conducted for SSL as the sole carbon source in bioprocesses. It has been demonstrated in this work that the fundamentals of carbon and DoR balances work for the waste stream media with a deviation of ± 10 %. This ensures a complete coverage of the most important influencing factors of processes based on SSL by measuring the biomass content, CO_2 and O_2 in the exhaust gas, sugars via HPLC and the organic acids via CEDEX.

An increase of the production rates are reported in literature for various of products under phosphate limiting conditions in different expression hosts, for example, bacteria [104, 105] or unicellular eukaryotes [106, 107]. The results of this study indicate that there is a similar behavior of the strain *C. glutamicum CR099::U pXMJ19-pedACD* for the production of pediocin PA-1.
In contrast, phosphate limiting conditions are reported to substantially reduce the growth of *C. glutamicum* in CGXII medium [108, 109]. On the other hand, higher sugar and nitrogen concentrations in the reaction broth are reported to have a beneficial affect on the growth of the cells [110]. However, the DoE showed no significant impact of these factors on the cell growth of the bacteria. This is due to the low growth rates in the induction phase caused by the increased metabolic burden on the cells for the formation of the product [101].

Model development of processes with *C. glutamicum* utilizing complex media with SSL addition could be successfully adapted to the performed experiments [53, 56, 57, 58]. Compared to the biomass yields from these processes, the yields of the batch are significant reduced to about half. One reason for this could be that another strain was used in this study. Besides the genes for the formation of pediocin PA-1, the strain has the genes for improved mannose and xylose uptake integrated into the genome rather than on plasmids which affects the physiology. Additionally, the growth of *C. glutamicum* is substantially reduced in the presence of furfural, an inhibitory compound of SSL [68]. As higher SSL concentrations were used in this work compared to the other studies, this would lead to decreased growth. Additionally, in models the inhibition is accounted for by inhibitory terms [53, 54]. However, the implementation of these terms showed no enhancement of the model with the given data.

As in the induced fed-batch the behavior of the cells deviated significantly from the batch, 2 different parameter sets were estimated. In fed-batch, the estimated $Y_{X/Si}$ parameters are substantially reduced compared to batch. One reason for this could be that the metabolic burden for the production of pediocin is affecting the growth rate in this phase [101].
Models of continuous processes of *C. glutamicum* based on complex media supplemented with SSL reached an NRMSE value below the acceptance criterion of 15 % for the states biomass, glucose, mannose and xylose [53, 58]. In contrast, the developed model in this work could met the criterion for mannose and xylose in batch as well as biomass, mannose and xylose in fed-batch. In the batch, the measured biomass measurements are affected by a high variability which impacts the correct prediction. For glucose, these inaccuracies of the biomass estimation influences the sugar estimation significantly, which hinders an accurate prediction of the state.

4 Conclusion and Outlook

Prior to this work, experiments of *C. glutamicum* on complex media supplemented with 5 - 10 % SSL were performed. Based on these experiments, the major goal of this study was to optimize the pediocin PA-1 titer of a bioprocess of *C. glutamicum CR099::U pXMJ19-pedACD* on SSL as the sole carbon source. It was demonstrated that the processes can be carried out without the need for complex media and the supplementation of trace elements or other additives except for a nitrogen and phosphate source. Comparable titers were obtained with a corresponding more economical and environmentally friendly process.

The central tasks of the thesis were as follows:
i) The experimental data should be assessed by examining the elemental (carbon, nitrogen and phosphorus) and electron balance.
ii) Based on a DoE approach, the influence of different SSL, nitrogen and phosphate availability on the product titer and on growth in the induction phase should be investigated.
iii) A mechanistic model should be set up based on the obtained knowledge in order to identify and model the underlying biological mechanisms of the cell.

Elemental Balance

The reliability of the experimental data was assessed by evaluating the elemental and electron balances over the course of the process. It was investigated, whether the corresponding ratios met the critical acceptance criterion of 10 %. Except for one experiment, the carbon and DoR balance met this criterion. Therefore it can be concluded, that no unknown components in the SSL were consumed or secreted as well as oxidized in significant amounts by the bacteria.
The nitrogen balance, however, showed that significant quantities of the elements were not recovered. The most likely explanation for this is that ammonia vitalizes through the exhaust gases, which leads to a significant underestimation of the nitrogen content. For the phosphorus balance, a simplification was met by the introduction of $Ca_3(PO)_4$ as a secondary component of the non-biomass DCW. The conducted calculation overestimates the quantities of phosphorus in the samples constantly, which indicates a systematic error. As the measured experimental data does not describe the

distribution of nitrogen and phosphorus within the reactor sufficiently, the data is not reliable and can not be implemented in the model. Therefore, a simplification was met for the description of the pediocin PA-1 formation by introducing the carbon to phosphate feed ratio as a constant over the fed-batch time.

Design of Experiment

The DoE showed no significant correlation of the factors on the growth of the bacterium during the induction phase. However, the phosphate concentration has a significant impact on the product titer in the reaction broth. It can be concluded that a reduction of phosphate availability for the cells in the induction phase favors the pediocin PA-1 formation of the bacterium. The maximum product titer was observed at the edge of the DoE, implying that the optimal production conditions were not covered by the design space. As the factors SSL and nitrogen have no influence on growth and pediocin PA-1 titer, the factors can be kept at the minimum values of the examined boundaries to ensure maximum economic viability.

Mechanistic Model

A mechanistic model was set up based on the studies of the experiments with a combination of complex media and SSL. For the verification of the model, an acceptance criterion of 15 % of the NRMSE values was set. In batch, the model was capable to accurately predict the uptake of mannose and xylose with an NRMSE of 2.68 and 3.28 %. However, the model failed to accurately simulate the biomass due to the high variability of the initial biomass concentration and the error range of the measurement. The NRMSE of glucose is 16.60 % and does not meet the acceptance criterion, which is caused by the significant impact of the inaccurate biomass prediction on the state. For acetate, measurement errors may be present in the lower concentration ranges which complicates the correct prediction and verification in batch.
In contrast, the model accurately predicted the growth of the bacterium in fed-batch as well as the sugar uptake of mannose and xylose throughout the processes. For glucose, the error rate is at approximately 57 % which reflects a low prediction quality for this state. An NRMSE of approximately 56 % was observed for acetate which was caused by the low concentrations range of organic acid. However, the NRMSE does not reflect the importance of the state as it has only a minor impact on the model and on the other states. Due to the inaccuracy of the assay for the determination of the pediocin PA-1 concentration, there is a high error margin of the predicted values, which complicates the identification as well as the verification of the correct mechanism of the product formation.

Summary and Outlook

It can be concluded that a process using *C. glutamicum* for the recombinant production of pediocin PA-1 on SSL could be successfully developed, which underlines the general feasibility of bioprocesses using SSL as a substrate. Furthermore, the carbon and

electron balance met the set acceptance criterion, which demonstrates that the fundamentals of balancing are valid for SSL. Additionally, it was shown that one potential screw to increase pediocin PA-1 titer in the process is the phosphate availability of the cells in the induction phase. In contrast, no significant impact was found of the factors on growth. Moreover, the models based on SSL in combination with complex media could be adapted to the performed experiments. The model was capable to predict observations mannose and xylose in batch as well as the growth, mannose, xylose and acetate in fed-batch.

One key factor to increase the profitability of the process is to enhance the pediocin PA-1 titer by finding the optimal process conditions. As the DoE did not capture the optimum of the pediocin PA-1 concentration, the boundaries of the design space should therefore be shifted to higher phosphate limitation. In order to increase the space-time yield of the process, the batch conditions could be further investigated to find the optimal growth conditions of the bacteria and to reduce the batch time. In contrast, an uninduced fed-batch would be another alternative for increasing the biomass concentration before the induction. In order to improve the overall batch prediction of the model, the variability of the initial biomass concentration has to be lowered by either increasing the starting biomass or reducing the error margin of the measurement. Acetate measurement may have problems in the lower concentration ranges which should be investigated by spiking acetate in SSL samples. Due to the nature of the pediocin assay and the corresponding inaccuracies, an accurate description of the pediocin formation and validation is difficult. This underlines the need for a new analytical technique, for example, HPLC or ELISA, in order to obtain more precise concentration values. Additionally, the specific product formation rate of the model is based on a simplification of the phosphate term since the phosphorus balance does not meet the critical acceptance criteria. As this simplification is unable to address a change in phosphate availability during the process, the discrepancies in the P-balance should be examined by analyzing the elemental composition of the precipitate.

With the increasing challenges posed by climate change, it is becoming more and more important to rethink the concepts of sustainability and resource friendliness. The biotechnology industry is a sector that can contribute significantly to this field. Currently, the cultivation of microorganisms is still mainly based on food crops. However, in terms of economically and ecologically sustainable process management, the trend is moving towards second generation feedstocks. The iFermenter project, to which this study contributes, aims to recycle the waste stream media SSL from the paper industry by the production of high-value bacteriocins with *C. glutamicum*. As a next step toward an industrial application, the bench-scale processes performed in this thesis should be upscaled and carried out in a pilot plant, which is currently in progress. The process could next be connected to the paper processing industry to recycle a significant amount of generated waste and introduce circular economy. Moreover, the process could act as a basis for the development of further high-value products.

References

[1] Wang Jiajing and Leping A N D Sun Hanlong Jiang. Early evidence for beer drinking in a 9000-year-old platform mound in southern China. *PLOS ONE*, 16(8):1–20, 10 2021.

[2] P L Rogers, Y J Jeon, and C J Svenson. Application of Biotechnology to Industrial Sustainability. *Process Safety and Environmental Protection*, 83(6):499–503, 2005.

[3] Giedrius Gasiunas, Rodolphe Barrangou, Philippe Horvath, and Virginijus Siksnys. Cas9–crRNA ribonucleoprotein complex mediates specific DNA cleavage for adaptive immunity in bacteria. *Proceedings of the National Academy of Sciences*, 109(39):E2579–E2586, 2012.

[4] Precedence Research. Biotechnology Market Size, Share, Growth, Forecast 2021-2030. Technical report, Precedence Research, 2020.

[5] John M Woodley. Towards the sustainable production of bulk-chemicals using biotechnology. *New Biotechnology*, 59:59–64, 2020.

[6] Byong H. Lee. Fundamentals and New Aspects. In *Fundamentals of Food Biotechnology*, chapter 1, pages 1–146. John Wiley & Sons, Ltd, 2015.

[7] Adilson José de Assis and Rubens Maciel Filho. Soft sensors development for on-line bioreactor state estimation. *Computers & Chemical Engineering*, 24(2):1099–1103, 2000.

[8] G Dünnebier and H Tups. FDA PAT Initiative – Eine Anwendersicht zu technischen Möglichkeiten und aktueller industrieller Umsetzung. *Chemie Ingenieur Technik*, 79(12):2019–2028, 2007.

[9] Johannes Möller and Ralf Pörtner. Model-Based Design of Process Strategies for Cell Culture Bioprocesses: State of the Art and New Perspectives. In Sivakumar Joghi Thatha Gowder, editor, *New Insights into Cell Culture Technology*, chapter 5. IntechOpen, Rijeka, 2017.

[10] Lenita Lindström-Gommers and Theresa Mullin. International Conference on Harmonization: Recent Reforms as a Driver of Global Regulatory Harmonization and Innovation in Medical Products. *Clinical Pharmacology & Therapeutics*, 105(4):926–931, 2019.

[11] PAT — A Framework for Innovative Pharmaceutical Development, Manufacturing, and Quality Assurance . Technical report, US Food and Drug Administration, 2004.

[12] Pharmaceutical Development Q8(R2). Technical report, International Conference on Harmonisation of Technical Requirements for Pharmaceuticals for Human Use, 2009.

[13] Paul Kroll, Alexandra Hofer, Sophia Ulonska, Julian Kager, and Christoph Herwig. Model-Based Methods in the Biopharmaceutical Process Lifecycle. *Pharmaceutical Research*, 34(12):2596–2613, 2017.

[14] Dörte Solle, Bernd Hitzmann, Christoph Herwig, Manuel Pereira Remelhe, Sophia Ulonska, Lynn Wuerth, Adrian Prata, and Thomas Steckenreiter. Between the Poles of Data-Driven and Mechanistic Modeling for Process Operation. *Chemie Ingenieur Technik*, 89(5):542–561, 2017.

[15] Peter A Vanrolleghem and Denis Dochain. Bioprocess Model Identification. In *Advanced Instrumentation, Data Interpretation, and Control of Biotechnological Processes*, pages 251–318. Springer-Science+Business Media, 1998.

[16] Peter Reichert. *Concepts underlying a computer program for the identification and simulation of aquatic systems*. Swiss Federal Institute for Environmental Science and Technology (EAWAG), 1994.

[17] Marie-Joëlle Rochet and Jean-Pierre Flandrois. Bacterial Strain Characterization Using Mathematical Modelling of Growth. *Zentralblatt für Bakteriologie*, 271(1):2–10, 1989.

[18] Johannes Möller, Kim Beatrice Kuchemüller, Tobias Steinmetz, Kirsten Koopmann, and Ralf Pörtner. Model-assisted Design of Experiments as a concept for knowledge-based bioprocess development. *Bioprocess and biosystems engineering*, 42(5):867–882, 2019.

[19] Patrick Wechselberger, Patrick Sagmeister, and Christoph Herwig. Real-time estimation of biomass and specific growth rate in physiologically variable recombinant fed-batch processes. *Bioprocess and Biosystems Engineering*, 36(9):1205–1218, 2013.

[20] Vincent Brunner, Manuel Siegl, Dominik Geier, and Thomas Becker. Challenges in the Development of Soft Sensors for Bioprocesses: A Critical Review. *Frontiers in Bioengineering and Biotechnology*, 9, 2021.

[21] Coleman Brosilow and Babu Joseph. *Techniques of Model-Based Control*. Prentice Hall PTR, New Jersey, 1 edition, 2002.

[22] Yu Luo, Varghese Kurian, and Babatunde A Ogunnaike. Bioprocess systems analysis, modeling, estimation, and control. *Current Opinion in Chemical Engineering*, 33:100705, 2021.

[23] Jelena Djuris and Zorica Djuric. Modeling in the quality by design environment: Regulatory requirements and recommendations for design space and control strategy appointment. *International Journal of Pharmaceutics*, 533(2):346–356, 2017.

[24] Carl F Craver. When mechanistic models explain. *Synthese*, 153(3):355–376, 2006.

[25] Gregory N Stephanopoulos, Aristos A Aristidou, and Jens Nielsen. CHAPTER 4 - Material Balances and Data Consistency. In Gregory N Stephanopoulos, Aristos A Aristidou, and Jens Nielsen, editors, *Metabolic Engineering*, pages 115–146. Academic Press, San Diego, 1998.

[26] Paul Kroll, Alexandra Hofer, Ines V Stelzer, and Christoph Herwig. Workflow to set up substantial target-oriented mechanistic process models in bioprocess engineering. *Process Biochemistry*, 62:24–36, 2017.

[27] Peter Sinner, Sven Daume, Christoph Herwig, and Julian Kager. Usage of Digital Twins Along a Typical Process Development Cycle. In *Advances in biochemical engineering/biotechnology*, volume 176. Springer Cham, 11 2020.

[28] Ólafur Ögmundarson, Sumesh Sukumara, Markus J Herrgård, and Peter Fantke. Combining Environmental and Economic Performance for Bioprocess Optimization. *Trends in Biotechnology*, 38(11):1203–1214, 2020.

[29] Yaser Dahman, Kashif Syed, Sarkar Begum, Pallavi Roy, and Banafsheh Mohtasebi. 14 - Biofuels: Their characteristics and analysis. In Deepak Verma, Elena Fortunati, Siddharth Jain, and Xiaolei Zhang, editors, *Biomass, Biopolymer-Based Materials, and Bioenergy*, Woodhead Publishing Series in Composites Science and Engineering, pages 277–325. Woodhead Publishing, 2019.

[30] S N Naik, Vaibhav V Goud, Prasant K Rout, and Ajay K Dalai. Production of first and second generation biofuels: A comprehensive review. *Renewable and Sustainable Energy Reviews*, 14(2):578–597, 2010.

[31] Miguel A Carriquiry, Xiaodong Du, and Govinda R Timilsina. Second generation biofuels: Economics and policies. *Energy Policy*, 39(7):4222–4234, 2011.

[32] Sarah C Davis, William J Parton, Stephen J Del Grosso, Cindy Keough, Ernest Marx, Paul R Adler, and Evan H DeLucia. Impact of second-generation biofuel agriculture on greenhouse-gas emissions in the corn-growing regions of the US. *Frontiers in Ecology and the Environment*, 10(2):69–74, 2012.

[33] European Commission, Directorate-General for Research, and Innovation. *Innovating for sustainable growth : a bioeconomy for Europe*. Publications Office, 2012.

[34] Anuj Kumar Chandel, Vijay Kumar Garlapati, Akhilesh Kumar Singh, Felipe Antonio Fernandes Antunes, and Silvio Silvério da Silva. The path forward for lignocellulose biorefineries: Bottlenecks, solutions, and perspective on commercialization. *Bioresource Technology*, 264:370–381, 2018.

[35] CEPI. CEPI Key Statistics European pulp & paper industry. Technical report, Confederation of European Paper Industries, 2021.

[36] Hugh G Lawford and Joyce D Rousseau. Production of ethanol from pulp mill hardwood and softwood spent sulfite liquors by genetically engineeredE. coli. *Applied Biochemistry and Biotechnology*, 39(1):667–685, 1993.

[37] C Rueda, J Fernández-Rodríguez, G Ruiz, T Llano, and A Coz. Monosaccharide production in an acid sulfite process: Kinetic modeling. *Carbohydrate Polymers*, 116:18–25, 2015.

[38] A Arkell, J Olsson, and O Wallberg. Process performance in lignin separation from softwood black liquor by membrane filtration. *Chemical Engineering Research and Design*, 92(9):1792–1800, 2014.

[39] Daniel LA Fernandes, Susana R Pereira, Luísa S Serafim, Dmitry V Evtuguin, and AMRB Xavier. Second generation bioethanol from lignocellulosics: processing of hardwood sulphite spent liquor. *Pinheiro Lima MA, editor. Bioethanol: InTech*, pages 123–152, 2012.

[40] Michaela Weissgram, Janina Gstöttner, Bettina Lorantfy, Raimund Tenhaken, Christoph Herwig, and Hedda K Weber. Generation of PHB from Spent Sulfite Liquor Using Halophilic Microorganisms. *Microorganisms*, 3(2):268–289, 2015.

[41] Steve S Helle, Tony Lin, and Sheldon J B Duff. Optimization of spent sulfite liquor fermentation. *Enzyme and Microbial Technology*, 42(3):259–264, 2008.

[42] Michaela Weissgram, Thomas Ters, Hedda K Weber, and Christoph Herwig. Investigating the potential of thermophilic species for ethanol production from industrial spent sulfite liquor. *AIMS Energy*, 3(4):592–611, 2015.

[43] S Y Lin. Commercial Spent Pulping Liquors. In Stephen Y Lin and Carlton W Dence, editors, *Methods in Lignin Chemistry*, pages 75–80. Springer Berlin Heidelberg, Berlin, Heidelberg, 1992.

[44] T Llano, M Alexandri, A Koutinas, Chr. Gardeli, H Papapostolou, A Coz, N Quijorna, A Andres, and M Komaitis. Liquid–Liquid Extraction of Phenolic Compounds from Spent Sulphite Liquor. *Waste and Biomass Valorization*, 6(6):1149–1159, 2015.

[45] Chrysanthi Pateraki, Dimitrios Ladakis, Lutgart Stragier, Willy Verstraete, Ioannis Kookos, Seraphim Papanikolaou, and Apostolis Koutinas. Pretreatment of spent sulphite liquor via ultrafiltration and nanofiltration for bio-based succinic acid production. *Journal of Biotechnology*, 233:95–105, 2016.

[46] J N Nigam. Ethanol production from hardwood spent sulfite liquor using an adapted strain of Pichia stipitis. *Journal of Industrial Microbiology and Biotechnology*, 26:145–150, 2001.

[47] Shiyuan Yu, Morris Wayman, and Sarad K Parekh. Fermentation to ethanol of pentose-containing spent sulphite liquor. *Biotechnology and Bioengineering*, 29(9):1144–1150, 1987.

[48] Demetri Petrides. BioProcess Design and Economics, 2nd Edition. In *Bioseparations Science and Engineering*, volume 2. Oxford University Press, 10 2015.

[49] Charlotte Anne Vees, Lukas Veiter, Fritz Sax, Christoph Herwig, and Stefan Pflügl. A robust flow cytometry-based biomass monitoring tool enables rapid at-line characterization of S. cerevisiae physiology during continuous bioprocessing of spent sulfite liquor. *Analytical and Bioanalytical Chemistry*, 412(9):2137–2149, 2020.

[50] Vera Novy, Stefan Krahulec, Karin Longus, Mario Klimacek, and Bernd Nidetzky. Co-fermentation of hexose and pentose sugars in a spent sulfite liquor matrix with genetically modified Saccharomyces cerevisiae. *Bioresource Technology*, 130:439–448, 2013.

[51] Yannick Bus. Development of a PAT strategy for renewable substrates to enable in-process control. *Master Thesis*, 2022.

[52] Daniel J Hayes, Steve Fitzpatrick, Michael H B Hayes, and Julian R H Ross. The Biofine Process – Production of Levulinic Acid, Furfural, and Formic Acid from Lignocellulosic Feedstocks. In *Biorefineries-Industrial Processes and Products*, chapter 7, pages 139–164. John Wiley & Sons, Ltd, 2005.

[53] Peter Sinner, Julian Kager, Sven Daume, and Christoph Herwig. Model-based Analysis and Optimisation of a Continuous Corynebacterium glutamicum Bioprocess Utilizing Lignocellulosic Waste. *IFAC-PapersOnLine*, 52(26):181–186, 2019.

[54] S Rousseau, Denis J Rouleau, Laleh Yerushalmi, and Raymond Mayer. Effect of temperature on fermentation kinetics of waste sulphite liquor by Saccharomyces cerevisiae. *Journal of Chemical Technology & Biotechnology*, 53:285–291, 2007.

[55] B F Safi, D Rouleau, R C Mayer, and M Desrochers. Fermentation kinetics of spent sulfite liquor by Saccharomyces cerevisiae. *Biotechnology and Bioengineering*, 28(7):944–951, 1986.

[56] Peter Sinner, Marlene Stiegler, Christoph Herwig, and Julian Kager. Noninvasive online monitoring of Corynebacterium glutamicum fed-batch bioprocesses subject to spent sulfite liquor raw material uncertainty. *Bioresource Technology*, 321:124395, 2021.

[57] Pedro A Lira-Parada, Peter Sinner, Michael Kohlstedt, Julian Kager, Christoph Wittmann, Christoph Herwig, and Nadav Bar. Linking process and metabolic modelling for the estimation of carbon flux distribution in Corynebacterium glutamicum growth in spent sulfite liquor. *IFAC-PapersOnLine*, 55(7):228–233, 2022.

[58] Peter Sinner, Marlene Stiegler, Oliver Goldbeck, Gerd M Seibold, Christoph Herwig, and Julian Kager. Online estimation of changing metabolic capacities in continuous Corynebacterium glutamicum cultivations growing on a complex sugar mixture. *Biotechnology and Bioengineering*, 119(2):575–590, 2022.

[59] Jong An Lee, Jung Ho Ahn, and Sang Yup Lee. 3.15 - Organic Acids: Succinic and Malic Acids. In Murray Moo-Young, editor, *Comprehensive Biotechnology (Third Edition)*, pages 172–187. Pergamon, Oxford, third edition edition, 2019.

[60] Nisarg Gohil, Gargi Bhattacharjee, and Vijai Singh. Chapter 1 - An introduction to microbial cell factories for production of biomolecules. In Vijai Singh, editor, *Microbial Cell Factories Engineering for Production of Biomolecules*, pages 1–19. Academic Press, 2021.

[61] Xiuxia Liu, Yankun Yang, Wei Zhang, Yang Sun, Feng Peng, Laura Jeffrey, Linda M Harvey, Brian T McNeil, and Zhonghu Bai. Expression of recombinant protein using Corynebacterium Glutamicum: progress, challenges and applications. *Critical Reviews in Biotechnology*, 36:652 – 664, 2016.

[62] Judith Becker, Christina Maria Rohles, and Christoph Wittmann. Metabolically engineered Corynebacterium glutamicum for bio-based production of chemicals, fuels, materials, and healthcare products. *Metabolic Engineering*, 50:122–141, 2018.

[63] Thomas Hermann. Industrial production of amino acids by coryneform bacteria. *Journal of Biotechnology*, 104(1):155–172, 2003.

[64] Hideo Kawaguchi, Alain A Vertès, Shohei Okino, Masayuki Inui, and Hideaki Yukawa. Engineering of a Xylose Metabolic Pathway in Corynebacterium glutamicum. *Applied and Environmental Microbiology*, 72(5):3418–3428, 2006.

[65] Miho Sasaki, Haruhiko Teramoto, Masayuki Inui, and Hideaki Yukawa. Identification of mannose uptake and catabolism genes in Corynebacterium glutamicum and genetic engineering for simultaneous utilization of mannose and glucose. *Applied Microbiology and Biotechnology*, 89(6):1905–1916, 2011.

[66] N Bayan, C Houssin, M Chami, and G Leblon. Mycomembrane and S-layer: two important structures of Corynebacterium glutamicum cell envelope with promising biotechnology applications. *Journal of Biotechnology*, 104(1):55–67, 2003.

[67] Kerui Lin, Shuangyan Han, and Suiping Zheng. Application of Corynebacterium glutamicum engineering display system in three generations of biorefinery. *Microbial Cell Factories*, 21(1):14, 2022.

[68] Yota Tsuge, Yoshimi Hori, Motonori Kudou, Jun Ishii, Tomohisa Hasunuma, and Akihiko Kondo. Detoxification of furfural in Corynebacterium glutamicum under aerobic and anaerobic conditions. *Applied Microbiology and Biotechnology*, 98(20):8675–8683, 2014.

[69] Roland Freudl. Beyond amino acids: Use of the Corynebacterium glutamicum cell factory for the secretion of heterologous proteins. *Journal of Biotechnology*, 258:101–109, 2017.

[70] Long Liu, Haiquan Yang, Hyun-dong Shin, Jianghua Li, Guocheng Du, and Jian Chen. Recent advances in recombinant protein expression by Corynebacterium, Brevibacterium, and Streptomyces: from transcription and translation regulation to secretion pathway selection. *Applied Microbiology and Biotechnology*, 97:9597 – 9608, 2013.

[71] Gian Maria Rossolini, Fabio Arena, Patrizia Pecile, and Simona Pollini. Update on the antibiotic resistance crisis. *Current Opinion in Pharmacology*, 18:56–60, 2014.

[72] Matthew I Hutchings, Andrew W Truman, and Barrie Wilkinson. Antibiotics: past, present and future. *Current Opinion in Microbiology*, 51:72–80, 2019.

[73] Maria Zimina, Olga Babich, Alexander Prosekov, Stanislav Sukhikh, Svetlana Ivanova, Margarita Shevchenko, and Svetlana Noskova. Overview of Global Trends in Classification, Methods of Preparation and Application of Bacteriocins. *Antibiotics*, 9(9), 2020.

[74] T M Karpiński and A K Szkaradkiewicz. Bacteriocins. In Benjamin Caballero, Paul M Finglas, and Fidel Toldrá, editors, *Encyclopedia of Food and Health*, pages 312–319. Academic Press, Oxford, 2016.

[75] Paweł Mak. Chapter 13 - Staphylococcal Bacteriocins. In Vincenzo Savini, editor, *Pet-To-Man Travelling Staphylococci*, pages 161–171. Academic Press, 2018.

[76] Lucy H Deegan, Paul D Cotter, Colin Hill, and Paul Ross. Bacteriocins: Biological tools for bio-preservation and shelf-life extension. *International Dairy Journal*, 16(9):1058–1071, 2006.

[77] R Lagos. Bacteriocins. In Stanley Maloy and Kelly Hughes, editors, *Brenner's Encyclopedia of Genetics (Second Edition)*, pages 277–279. Academic Press, San Diego, second edition edition, 2013.

[78] Paul D Cotter, R Paul Ross, and Colin Hill. Bacteriocins — a viable alternative to antibiotics? *Nature Reviews Microbiology*, 11(2):95–105, 2013.

[79] Veeresh Juturu and Jin Chuan Wu. Microbial production of bacteriocins: Latest research development and applications. *Biotechnology Advances*, 36(8):2187–2200, 2018.

[80] M P Zacharof and R W Lovitt. Bacteriocins Produced by Lactic Acid Bacteria a Review Article. *APCBEE Procedia*, 2:50–56, 2012.

[81] Eluned Jones, Victoria Salin, and Gary W Williams. NISIN AND THE MARKET FOR COMMERICIAL BACTERIOCINS. Technical report, 2005.

[82] Lars Mogren, Sofia Windstam, Sofia Boqvist, Ivar Vågsholm, Karin Söderqvist, Anna K Rosberg, Julia Lindén, Emina Mulaosmanovic, Maria Karlsson, Elisabeth Uhlig, Åsa Håkansson, and Beatrix Alsanius. The Hurdle Approach–A Holistic Concept for Controlling Food Safety Risks Associated With Pathogenic Bacterial Contamination of Leafy Green Vegetables. A Review. *Frontiers in Microbiology*, 9, 2018.

[83] Triona O'Keeffe and Colin Hill. BACTERIOCINS | Potential in Food Preservation. In Richard K Robinson, editor, *Encyclopedia of Food Microbiology*, pages 183–191. Elsevier, Oxford, 1999.

[84] Sahar Abbasiliasi, Tan Joo Shun, Tengku Ibrahim, Fatemeh Bashokouh, Ramakrishnan Nagasundara Ramanan, Mustafa Shuhaimi, and Arbakariya Ariff. Fermentation factors influencing the production of bacteriocins by lactic acid bacteria: A review. *RSC Adv.*, 7:29395–29420, 10 2017.

[85] J M Rodrı́guez, M I Martı́nez, N Horn, and H M Dodd. Heterologous production of bacteriocins by lactic acid bacteria. *International Journal of Food Microbiology*, 80(2):101–116, 2003.

[86] Oliver Goldbeck, Dominique N Desef, Kirill V Ovchinnikov, Fernando Perez-Garcia, Jens Christmann, Peter Sinner, Peter Crauwels, Dominik Weixler, Peng Cao, Judith Becker, Michael Kohlstedt, Julian Kager, Bernhard J Eikmanns, Gerd M Seibold, Christoph Herwig, Christoph Wittmann, Nadav S Bar, Dzung B Diep, and Christian U Riedel. Establishing recombinant production of pediocin PA-1 in Corynebacterium glutamicum. *Metabolic Engineering*, 68:34–45, 2021.

[87] Maria Carolina W Porto, Taís Mayumi Kuniyoshi, P O S Azevedo, Michele Vitolo, and R P S Oliveira. Pediococcus spp.: An important genus of lactic acid bacteria and pediocin producers. *Biotechnology Advances*, 35(3):361–374, 2017.

[88] Line Johnsen, Gunnar Fimland, Vincent Eijsink, and Jon Nissen-Meyer. Engineering Increased Stability in the Antimicrobial Peptide Pediocin PA-1. *Applied and Environmental Microbiology*, 66(11):4798–4802, 2000.

[89] M B Cole, M V Jones, and C Holyoak. The effect of pH, salt concentration and temperature on the survival and growth of Listeria monocytogenes. *Journal of Applied Bacteriology*, 69(1):63–72, 1990.

[90] Nassra Dabour, Annina Zihler, Ehab Kheadr, Christophe Lacroix, and Ismail Fliss. In vivo study on the effectiveness of pediocin PA-1 and Pediococcus acidilactici UL5 at inhibiting Listeria monocytogenes. *International Journal of Food Microbiology*, 133(3):225–233, 2009.

[91] Paul Mead, Laurence Slutsker, Vance Dietz, Linda Mccaig, Joseph Bresee, Craig Shapiro, Patricia Griffin, and Robert Tauxe. Food-Related Illness and Death in the United States. *Emerging infectious diseases*, 5:607–625, 12 1999.

[92] G Le Blay, C Lacroix, A Zihler, and I Fliss. In vitro inhibition activity of nisin A, nisin Z, pediocin PA-1 and antibiotics against common intestinal bacteria. *Letters in Applied Microbiology*, 45(3):252–257, 2007.

[93] Lucie Beaulieu, Dmitri Tolkatchev, Jean-François Jetté, and Muriel Subirade. Production of active pediocin PA-1 in Escherichia coli using a thioredoxin gene fusion expression approach. *Canadian journal of microbiology*, 53:1246–1258, 12 2007.

[94] Matthias Ruwe, Jörn Kalinowski, and Marcus Persicke. Identification and Functional Characterization of Small Alarmone Synthetases in Corynebacterium glutamicum. *Frontiers in Microbiology*, 8, 2017.

[95] Marten Linder, Markus Haak, Angela Botes, Jörn Kalinowski, and Christian Rückert. Construction of an IS-Free Corynebacterium glutamicum ATCC 13 032 Chassis Strain and Random Mutagenesis Using the Endogenous ISCg1 Transposase. *Frontiers in Bioengineering and Biotechnology*, 9:751334, 2021.

[96] J D Marugg, C F Gonzalez, B S Kunka, A M Ledeboer, M J Pucci, M Y Toonen, S A Walker, L C Zoetmulder, and P A Vandenbergh. Cloning, expression, and nucleotide sequence of genes involved in production of pediocin PA-1, and bacteriocin from Pediococcus acidilactici PAC1.0. *Applied and Environmental Microbiology*, 58(8):2360–2367, 1992.

[97] Julian Kager, Andrea Tuveri, Sophia Ulonska, Paul Kroll, and Christoph Herwig. Experimental verification and comparison of model predictive, PID and model inversion control in a Penicillium chrysogenum fed-batch process. *Process Biochemistry*, 90:1–11, 2020.

[98] Roland Brun, Martin Kühni, Hansruedi Siegrist, Willi Gujer, and Peter Reichert. Practical identifiability of ASM2d parameters—systematic selection and tuning of parameter subsets. *Water Research*, 36(16):4113–4127, 2002.

[99] SIMON BARRY and JANE ELITH. Error and uncertainty in habitat models. *Journal of Applied Ecology*, 43(3):413–423, 2006.

[100] Roche. *Manual CEDEX Bio HT Analyzer*. Roche, 2015.

[101] WE Bentley and DS Kompala. A novel structured kinetic modeling approach for the analysis of plasmid instability in recombinant bacterial cultures. *Biotechnol Bioeng*, 33:49–61, 1989.

[102] J R Freney, J R Simpson, and O T Denmead. AMMONIA VOLATILIZATION. *Ecological Bulletins*, pages 291–302, 1981.

[103] Philippe Dantigny. Modeling of the aerobic growth of Saccharomyces cerevisiae on mixtures of glucose and ethanol in continuous culture. *Journal of Biotechnology*, 43(3):213–220, 1995.

[104] Lu Zhang, Leshi Liu, Ke-Feng Wang, Lan Xu, Liming Zhou, Weishan Wang, Chuan Li, Zheng Xu, Tong Shi, Haihong Chen, Yuanhang Li, Hui Xu, XiuLiang Yang, Zhichun Zhu, Biqin Chen, Dan Li, Guanghuang Zhan, Si-Liang Zhang, Li-Xin Zhang, and Gao-Yi Tan. Phosphate limitation increases coenzyme Q10 production in industrial Rhodobacter sphaeroides HY01. *Synthetic and Systems Biotechnology*, 4(4):212–219, 2019.

[105] K G Clarke, F Ballot, and S J Reid. Enhanced rhamnolipid production by Pseudomonas aeruginosa under phosphate limitation. *World Journal of Microbiology and Biotechnology*, 26(12):2179–2184, 2010.

[106] Youlian Pan, Durvasula V Subba Rao, and Kenneth H Mann. CHANGES IN DOMOIC ACID PRODUCTION AND CELLULAR CHEMICAL COMPOSITION OF THE TOXIGENIC DIATOM PSEUDO-NITZSCHIA MULTISERIES UNDER PHOSPHATE LIMITATION1. *Journal of Phycology*, 32(3):371–381, 1996.

[107] Siguo Wu, Cuimin Hu, Guojie Jin, Xin Zhao, and Zongbao K Zhao. Phosphate-limitation mediated lipid production by Rhodosporidium toruloides. *Bioresource Technology*, 101(15):6124–6129, 2010.

[108] Takeru Ishige, Malgorzata Krause, Michael Bott, Volker F Wendisch, and Hermann Sahm. The Phosphate Starvation Stimulon of Corynebacterium glutamicum Determined by DNA Microarray Analyses. *Journal of Bacteriology*, 185(15):4519–4529, 2003.

[109] Martina Kočan, Steffen Schaffer, Takeru Ishige, Ulrike Sorger-Herrmann, Volker F Wendisch, and Michael Bott. Two-Component Systems of Corynebacterium glutamicum: Deletion Analysis and Involvement of the PhoS-PhoR System in the Phosphate Starvation Response. *Journal of Bacteriology*, 188(2):724–732, 2006.

[110] Fredrik Demoling, Daniela Figueroa, and Erland Bååth. Comparison of factors limiting bacterial growth in different soils. *Soil Biology and Biochemistry*, 39(10):2485–2495, 2007.

List of Figures

List of Tables